RESEARCH ON

DIGITAL TRANSDUCER PRINCIPLES

Final Report Vol. I

A PROPOSED MAGNETIC DIGITAL TEMPERATURE TRANSDUCER

by

Theodore E. Collier

Dimiter I. Tchernev

William H. Hartwig

September 30, 1972

for the

NATIONAL AERONAUTICS AND SPACE ADMINISTRATION

GRANT NGL-44-012-043

Department of Electrical Engineering

THE UNIVERSITY OF TEXAS AT AUSTIN

Austin, Texas 78712

Page Intentionally Left Blank

PREFACE

It has been known for many years that magnetic materials lose their magnetic properties at a temperature called the Curie temperature. An initial examination of this effect showed it had been used in temperature sensing by an analog application by K. Murakami[1] in 1964 and there are commercial products that use this effect to reduce the magnetic reluctance of relay and solenoid devices. As a preliminary program of research, it was decided to investigate the various magnetic properties to determine how materials might be characterized and synthesized. This volume of the Final Report is a detailed account of the project. It was completed in May 1970 as a Master's Degree thesis.

1. K. Murakami, "The Characteristics of Ferrite Cores with Low Curie Temperature and their Application," IEEE Trans Mag., June 1965, pp 96-100.

ABSTRACT

A study has been made of the feasibility of using the discontinuous permeability versus temperature characteristics of some magnetic materials for a digital temperature transducer and a thermally controlled ON-OFF switch. In the latter application, the AC impedance of a toroidal inductor was used as an ON-OFF switch in series with a load. Below the transition temperature the inductance (and impedance) are high and the switch is OFF, while above the transition temperature the inductance goes to zero and the switch is ON. This AC impedance switch is approaching the ultimate in reliability because of its simplicity (consisting only of a magnetic core and wire), shock and vibration insensitivity, radiation resistance, lack of moving parts and stability with time. In the former application, a string of cores with Curie temperatures spaced at a given interval are interrogated by a current input. The number of output pulses corresponds to the number of cores in the magnetic state. Simple logic converts the number of output pulse to a digital word recognizable by the system.

We have concentrated our efforts on materials with Curie temperatures between 0 and 100°C. One compound has the composition $Mn_{5-x}Fe_xGe_3$ where the amount of iron determines the transition temperature. The other compound is Ni-Zn ferrite and has the composition $Ni_{1-x}Zn_xFe_{1.95}O_4$, where the nickel: zinc ratio determines the transition temperature. A detailed report of materials prepared is presented. We have constructed toroidal inductors of the material and measured the change in inductance with temperature.

In view of these initial measurements, it is felt that a transducer utilizing the permeability versus temperature characteristics of these materials has promise as a reliable and sensitive solid state digital temperature transducer.

TABLE OF CONTENTS

LIST OF FIGURES

I. THEORY

A. INTRODUCTION AND CLASSIFICATION OF MAGNETIC MATERIALS

Magnetic materials can be classified into five major categories according to magnetic behavior:

1. Diamagnetic;
2. Paramagnetic;
3. Ferromagnetic;
4. Antiferromagnetic;
5. Ferrimagnetic.

The three parameters which describe the magnetic behavior of a material are: the magnetic field intensity H, the magnetic flux density B, and the magnetization M[1]. For a toroid or long solenoid

$$B = \mu_0(H + M) \text{ weber/m}^2$$

where μ_0 is the permeability of free space in henrys per meter. Also

$$B = \mu H = \mu_0 \mu_r H$$

where μ is the permeability of the material and μ_r is the relative permeability $(\frac{\mu}{\mu_0})$. The magnetization is related to the field by

$$M = \chi H$$

where χ is the magnetic susceptibility. The macroscopic magnetization M is defined as the average density per unit volume of the magnetic moments in a given direction. It should be noted that the magnetic parameters introduced above are vector quantities. The magnetization M is not necessarily coincident in direction with and proportional to the external field. If the magnetic vectors are not parallel, the relationship between B and H must be expressed with the aid of a permeability tensor $\tilde{\mu}$. Similarly, M is related to H through the susceptibility tensor $\tilde{\chi}$. For the materials presented in this paper, χ and μ reduce to scalar quantities.

A diamagnetic substance is unique due to the fact that its susceptibility is negative because the induced magnetic moment always opposes the applied field. There is no moment arising from the electron spin or orbital motions, therefore, diamagnetism occurs through a deformation of the electric charge distribution when a field is applied and disappears when the field is removed. The susceptibility is usually very small (-10^{-3} to -10^{-4}) compared to paramagnetic and ferromagnetic susceptibilities[2], and is of little importance in this report.

In a paramagnetic material, the individual atoms possess magnetic moments[3]. In contrast to diamagnetic materials, permanent magnetic dipoles exist in substances whose constituent ions or atoms have incomplete shells so that they possess some uncancelled orbital momentum and unpaired spins. The magnetic dipoles of paramagnetic materials are randomly oriented in the absence of an applied field and there is no net magnetization in any given direction. When a field is applied, the effect is to turn the dipoles slightly in the direction of the field so that statistically there are more dipoles pointing in the direction of B than in the opposite direction. The susceptibility is positive and small ($\sim 10^{-2}$ to 10^{-1}), but thermal agitation of the dipoles prevails and they are only partially aligned with the applied field[4].

The magnetic dipole moments in a ferromagnetic material are strongly aligned in the same direction. As a result, a spontaneous magnetization exists, that is, even in the absence of an applied field there is a magnetic moment. Weiss[5] postulated that the alignment is due to a strong interaction between the atomic dipoles, called the molecular or Weiss field. This interaction is of quantum-mechanical nature and is assumed proportional to the magnetization. The dipole alignment is temperature dependent since thermal

agitation increases as temperature increases. As a result, the spontaneous magnetization is temperature dependent. As long as the molecular field is strong enough to compete with this thermal agitation, the alignment remains and the material is still ferromagnetic. However, as temperature increases, thermal motion dominates and fewer dipoles are aligned. At a critical temperature called the Curie temperature, dipole alignment disappears and the material becomes paramagnetic. Above the Curie point, the susceptibility obeys the Curie-Weiss law, which states that $\frac{1}{\chi}$ rises from zero at the Curie point and increases linearly with temperature.

The fact that a ferromagnetic material may show no external evidence of being magnetized in spite of the spontaneous magnetization present led to the postulation of small regions called domains. In these regions (Weiss domains) there is a uniform magnetization, but the directions of the magnetization vectors are such that cancellation occurs with no externally applied field. When a field is applied, the magnetization process occurs either by rotation of the direction of the magnetization in the domains (domain rotation) or by motion of the walls separating the domains. The process of reorientation of the vectors is accomplished with a much smaller field strength than in a paramagnetic substance.

The simplest ferrimagnetic material is composed of two interpenetrating lattices, each sublattice being ferromagnetic[6]. Systems with more than two sublattices may occur, but the molecular field theory for a two sublattice system predicts the main features observed for the majority of known ferrimagnetic materials. The materials under discussion here are composed of two magnetic sublattices, commonly referred to as sublattices A and B. If the sublattices are occupied by identical ions and are antiparallel, the resultant moment will be zero ($M_A = M_B$) and the material is

said to be antiferromagnetic. The case of interest here is when there is a net moment ($M_A \neq M_B$) giving rise to ferrimagnetism.

B. Mn_5Ge_3

The phase diagram of the binary alloy system of manganese-germanium was investigated in detail by Zwicker, et al.[7] According to them, there exist four intermetallic compounds in this system: $Mn_{3.25}Ge$, Mn_5Ge_2, Mn_5Ge_3, and Mn_3Ge_2. The compound Mn_5Ge_3 (37.5 at % Ge) is formed at 932°C and forms solid solutions with appreciable amounts of manganese. In their study of this system, Zwicker, Jahn and Schubert[7] noted that Mn_5Ge_2 and Mn_5Ge_3 are strongly ferromagnetic. On the basis of this, it was suggested that the phases of composition intermediate between Mn_5Ge_2 and Mn_5Ge_3, i.e., alloys in the 28.6 to 37.5 at % germanium concentration level interval, must also be ferromagnetic. No other ferromagnetic alloys were found in this system.

The crystal structure of Mn_5Ge_3 was first identified by Castelliz[8], who showed that the Debye diagram can be satisfactorily explained by assuming a hexagonal $D8_8$ (Mn_5Si_3) type of structure. The lattice parameters were determined to be: a = 7.18 Å, c = 5.03 Å, and c/a = 0.701 at room temperature. The structure of $D8_8$ type is illustrated in Figure I-1, and the atomic positions are as follows:

4d (Mn)	1/3, 2/3, 0; 2/3, 1/3, 0;
	1/3, 2/3, 1/2; 2/3, 1/3, 1/2;
6g (Mn)	x, 0, 1/4; 0, x, 1/4;
	$\bar{x}$, $\bar{x}$, 1/4; $\bar{x}$, 0, 3/4;
	0, $\bar{x}$, 3/4; x, x, 3/4;
6g (Ge)	as above,

where x ≈ 0.6 in 6(g) metal site, and x ≈ 0.25 in metalloid site.

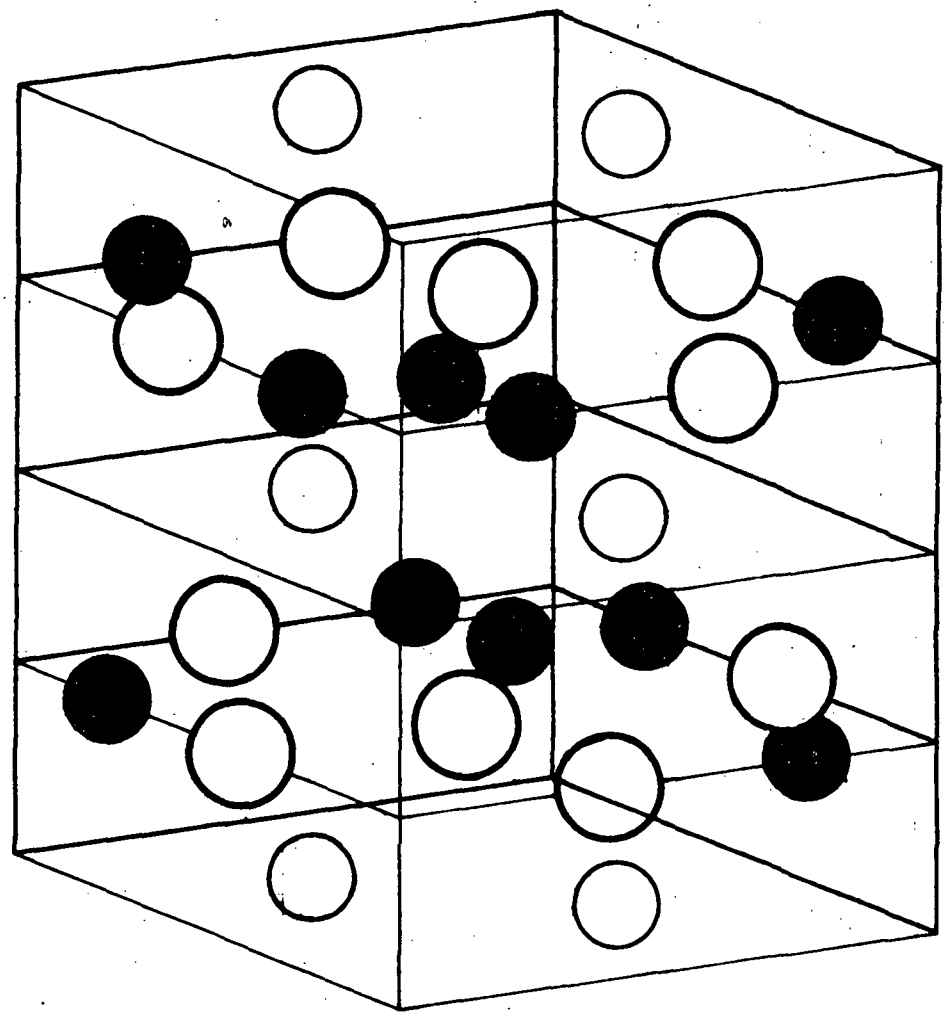

Figure I-1 Crystal structure of $D8_8$ type. Small closed circle: Iron group element. 4(d) site (A sublattice). Open small circle: Iron group element 6(g) site (B sublattice). Open large circle: IVb group element. 6(g) site.

Analyzing the experimental data on the structure and magnetic properties of alloys of manganese with elements of the fourth and fifth subgroups of periodic table, Guilland[9] noted that antiferromagnetic interaction occurs in these compounds when the separation between manganese ions located in the same magnetic sublattice (Mn_A - Mn_A) is smaller than the distance between manganese ions composing two different sublattices (Mn_A - Mn_B). At the same time, the Mn_A - Mn_B distance must not exceed the critical value of 2.81 Å, above which ferromagnetism occurs. According to Castelliz, the Mn_A - Mn_B distance for the Mn_5Ge_3 alloy is 3.08 Å which indicates that antiferromagnetic interaction cannot occur in this compound.

In a later study, Reiff, Steinfink and Narasimhan[10] investigated the magnetic behavior of the system $Mn_{5-x}Fe_xGe_3$, $0 \leq x \leq 2$, in an attempt to gain insight into the mechanism involved in the substitution of iron in the two sublattices, 4d and 6g. An analysis of the Mossbauer and magnetic measurements revealed that the initial iron substitution occurs in the 4(d) crystallographic sites of the $D8_8$ structure. When half of those sites are filled, additional iron goes into the 6(g) sites. They postulated a magnetic structure consisting of ferromagnetic alignment of spins within the two sublattices and antiparallel alignment between them. The Curie temperatures of $Mn_{5-x}Fe_xGe_3$ for x = 0, 0.5, 1.0, 1.5 were revealed to be 304, 318, 322, and 322°K, respectively.

The structure of Mn_5Ge_3 is $D8_8$, but the structure of Fe_5Ge_3 is the hexagonal $B8_2$ type, therefore, the extent of solid solution in the Mn-Fe-Ge system will be limited. Single phase material was observed by Reiff, et al. for all cases, except at the composition corresponding to x = 2, where several phases were present.

Because the hexagonal crystal has uniaxial symmetry, we expected the magnetic properties of Mn_5Ge_3 to be uniaxial. Tawara and Sato[11] claim the direction of easy magnetization lies along the c-axis. We found this was not the case (see Chapter III).

C. FERRITES

1. Crystal Structure

The best known ferrimagnetic materials are black, ceramic-like substances called ferrites. Ferrites, generally, have the chemical formula $MO\ Fe_2O_3$, where M is a divalent ion such as iron, nickel, zinc, copper, manganese, magnesium, aluminum, cobalt, or a combination of these[12]. The crystal structure as shown in Figure I-2 is that of the mineral spinel, $MgAl_2O_4$. The spinel structure is determined primarily by the oxygen ions lattice. The oxygen ions are larger than the metallic ions in the compound and form a face-centered cubic lattice. Consequently, the structure can be thought of as closely packed layers of oxygen ions, with the metallic ions occupying the interstices. A large number of different metallic ions can occur in the spinel, the primary requirement being that they are small enough so that the oxygen ions are not spread too far apart[13].

Within this lattice, two types of interstitial positions occur, denoted by A and B. Site A is known as a tetrahedral site and the metallic ion is surrounded by four oxygen ions. The metallic ion in the B site is enclosed by six oxygen ions of octahedral coordination. The unit cell of the cubic ferrite consists of eight ($MO\ Fe_2O_3$) units[14]. The geometric arrangement of the 32 oxygen ions results in 96 sites, 64 being tetrahedral and 32 octahedral. Of these 16 B sites and 8 A sites are occupied per unit cell. In Figure I-2, there are two groups of four cubes (octants). The ionic positions are the same in two octants sharing an edge and different in two

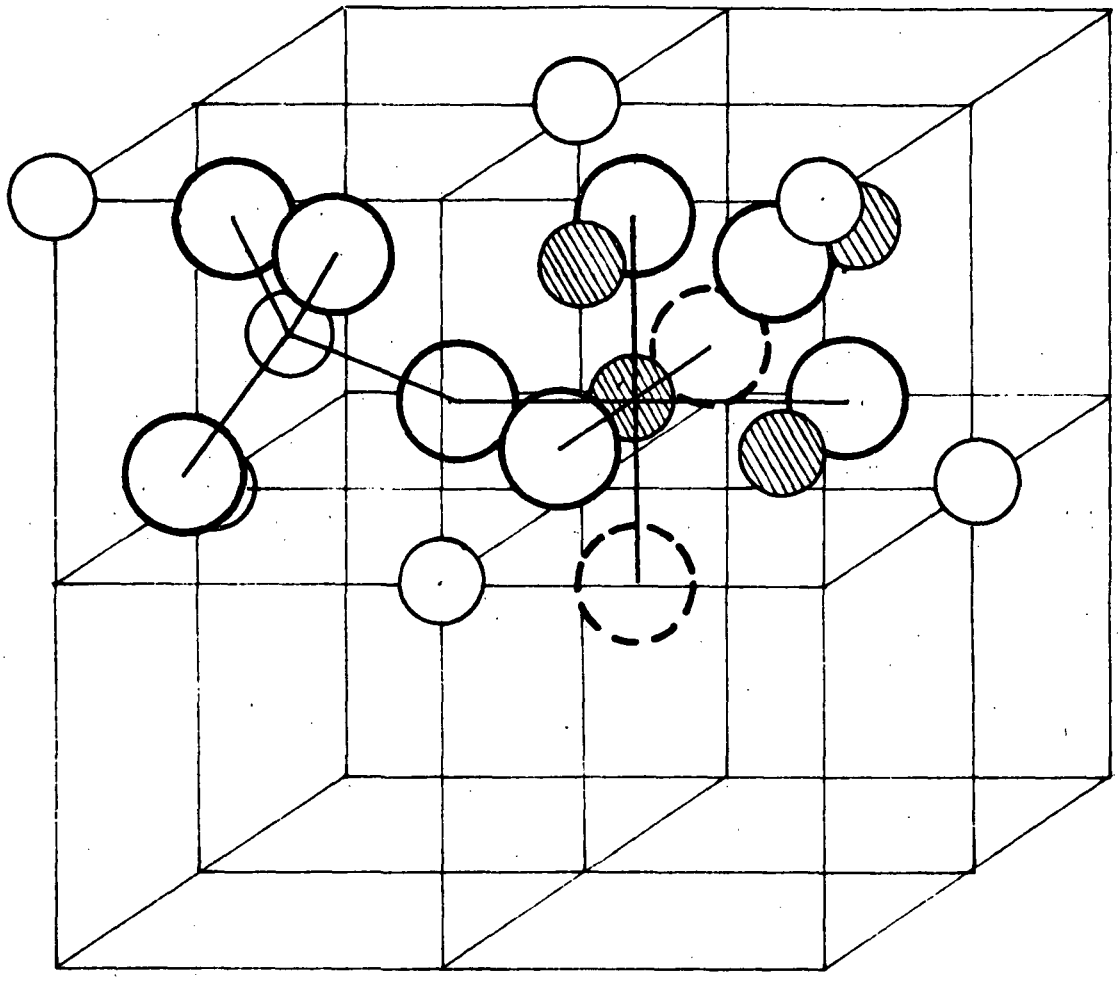

Figure I-2 Unit cell of the Spinel structure. Large sphere: oxygen ions. Small sphere, not shaded: metal ion in A site. Small sphere, shaded: metal ion in B site.

octants sharing a face or corner. Therefore, it is necessary only to show the positions of the ions in two adjacent octants to give a clear picture of the structure. Note that each octant contains four oxygen ions (large spheres) on the body diagonals of the octants and lying at the corners of a tetrahedron. The left-hand octant contains, in the center, a metal ion (small sphere, not shaded) surrounded by the tetrahedron of oxygen ions; this ion is said to occupy an A site. The right-hand octant shows four metal ions (small shaded spheres) each surrounded by an octahedron (one of which is shown) formed by six oxygen ions. Such ions are said to occupy B sites.

The magnetic properties of ferrites depend on how the metallic ions are distributed among the different sites[15]. The divalent ions commonly used in ferrites can be classified roughly into those preferring A sites (i.e., zinc) and those occupying B sites (nickel). In the normal spinel, the eight divalent ions go into the A sites and the sixteen trivalent ions enter the B sites. If the divalent ions prefer the B sites, then eight of the trivalent ions will be displaced and will enter the A sites. This is commonly referred to as an inverted spinel. There are also materials (Mg ferrite for example) which are partially inverted, but this is beyond the scope of this report.

A ferrite crystal has a domain structure similar to that of ferromagnetic metals. The magnetic moments of the constituent atoms determine the spontaneous saturation of the domains. The free oxygen atom has an incompleted 2P sub-shell, but the shell is filled when two electrons are acquired and it becomes an O^{2-} anion which is diamagnetic. Therefore, there is no magnetic moment associated with the oxygen atom, and it makes no direct contribution to the saturation value of the domain. The remaining ions have a magnetic moment as a result of unfilled outer sub-shells. The

magnetic moments due to the orbital motion of the electrons are quenched by internal fields. In other words, they are not oriented by externally applied fields[16]. The ionic magnetic moments are, therefore, due to parallel uncompensated electron spins in the ions. The free iron atom has an electronic configuration of $1S^2 2S^2 2P^6 3S^2 3P^6 3d^6 4S^2$. As defined by Hunds rule, there are four uncompensated spins in the 3d sub-shell. Therefore, if orbital quenching is assumed, the iron atom has a magnetic moment of four Bohr magnetoms ($4\mu_B$) due to spin. For Fe^{2+}, two electrons are lost from the 4S shell, and the resulting magnetic moment is still $4\mu_B$. In the case of the trivalent ion Fe^{3+}, one additional electron with negative spin in 3d is lost, and the magnetic moment becomes $5\mu_B$.

2. Superexchange Interaction

Strong quantum mechanical forces occur between neighboring metallic ions via intermediate oxygen atoms. This superexchange interaction is greatest if the three ions are collinear and if their separations are not too great[17]. The ion pair arrangements in the spinel that are important for this interaction are illustrated in Figure I-3. According to Neel[18], this interaction is negative in ferrites. As a result, the forces act to hold the neighboring atomic magnetic axes antiparallel. In contrast, the interaction is positive in ferromagnetic materials and the axes are aligned parallel. Three sets of forces exist in ferrites as depicted in Figure I-3. They may be classified as those between ions at the A sites, those between ions at the B sites, and also between A and B ions. This is commonly referred to as interactions A-A, B-B and A-B, respectively. For the A-B interaction shown in Figure I-3a, the angle and distances between ions are most favorable for superexchange. For the other cases, either the angle (Figure I-3a), one distance (Figures I-3b,d), or both (Figure I-3c) are

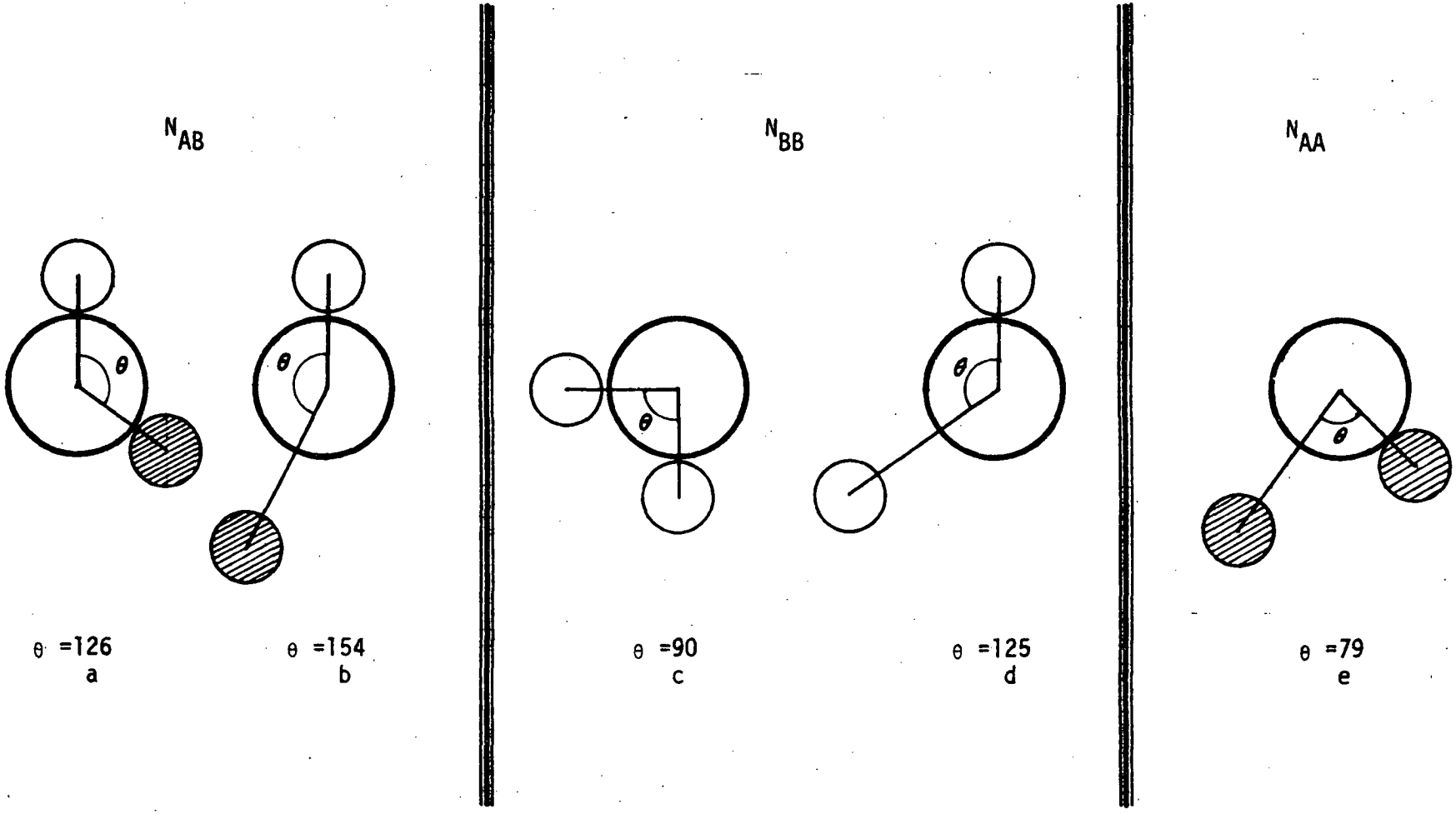

Figure I-3 Sketch of ion-pair configurations important for superexchange interaction. Large spheres represent oxygen ions, small crosshatched ones, cations in A sites, small light ones, cations in B sites. (After E. W. Gorter[19])

unfavorable. It may be concluded that the interaction between sublattices is stronger than those within the sublattices and that the A-A interaction is weakest of all. In addition, the negative A-B interaction shown in Figure I-3a predominates. This result supports the assumption that the magnetic axes of the A and B ions are held antiparallel to one another[19].

The spontaneous saturation magnetization of the domain is therefore due to the difference of the ionic moments on the A and B sites. For the inverse spinel arrangement described below, there are equal numbers of trivalent ions at each site which cancel out magnetically. As a result, the total moment per molecule is due to the divalent ion present.

As previously mentioned, zinc ferrites have the normal spinel structure. The zinc atoms occupy the A sites and have no magnetic moment. There are, therefore, no A-A or A-B interactions. At the B sites, however, there are iron ions each with a magnetic moment of $5\mu_B$. The condition known as antiferromagnetism should exist since only the negative B-B interaction remains. There are equal and opposite sets of magnetic ions resulting in a zero net magnetic moment. However, probably because the B-B interaction is weak, the antiferromagnetic condition has not been observed in zinc ferrite and it appears to be paramagnetic[20]. Nickel ferrite crystallizes into the inverse spinel arrangement and has a net magnetic moment, i.e., the material is ferrimagnetic.

3. Mixed Ferrites

Many improved magnetic properties have been found in mixed ferrites, which are solid solutions of two or more ferrites. Mixed ferrites are not confined to mixtures of inverse or normal with normal crystals. Nickel-zinc ferrite is an example of an inverse normal combination. This combination can be represented by the formula $(Zn_x^{2+}\ Fe_{1-x}^{3+})\ (Ni_{1-x}^{2+}\ Fe_{1+x}^{3+})O_4^{2-}$, where

the first pair of brackets enclose ions on the A sites and the second pair, ions at the B sites, and x may vary from zero to one. Assuming the prevalent interaction is a negative A-B interaction and that the iron has a theoretical moment of $5\mu_B$ and the zinc zero moment, the resultant moment per formula unit will be

$$\mu = -5(1 - x) + m(1 - x) + 5(1 + x)$$

$$\mu = 10x + m(1 - x) = (8x + 2)\ \mu_B$$

where m = 2 for Ni^{2+}. This relation is shown by the dotted line in Figure I-4. While this relation may be expected to hold for small values of x, it cannot do so when x approaches unity. For if x = 1, the ferrite is a simple zinc ferrite of normal spinel structure in which only the negative B-B interactions are expected and it has no ferrimagnetic properties. The substitution of zinc which prefers the A sites, upsets the ferric balance. The first effect of the addition of zinc is to increase the saturation magnetization. This is due, first, to the fact that when a nonmagnetic zinc ion enters a tetrahedral site, it displaces an Fe^{3+} ion so there is no longer a complete cancellation of the moments of the iron ions on octahedral sites by those on tetrahedral sites. The unbalanced ferric moments add to those of the Ni^{2+} ions. Also, the displaced Fe^{3+} ion will enter the B sublattice and take the place of the displaced Ni^{2+} ion. Since the Fe^{3+} has the larger moment, this too increases the saturation magnetization. As additional zinc ions enter the lattice, the reduced number of Fe^{3+} ions at the A sites become less able to maintain the alignment of the B sublattice against the B-B interaction. The alignment becomes progressively worse and the saturation moment eventually decreases. The observed decrease in Curie temperature as zinc concentration increases also suggests a decrease in the A-B interaction[21].

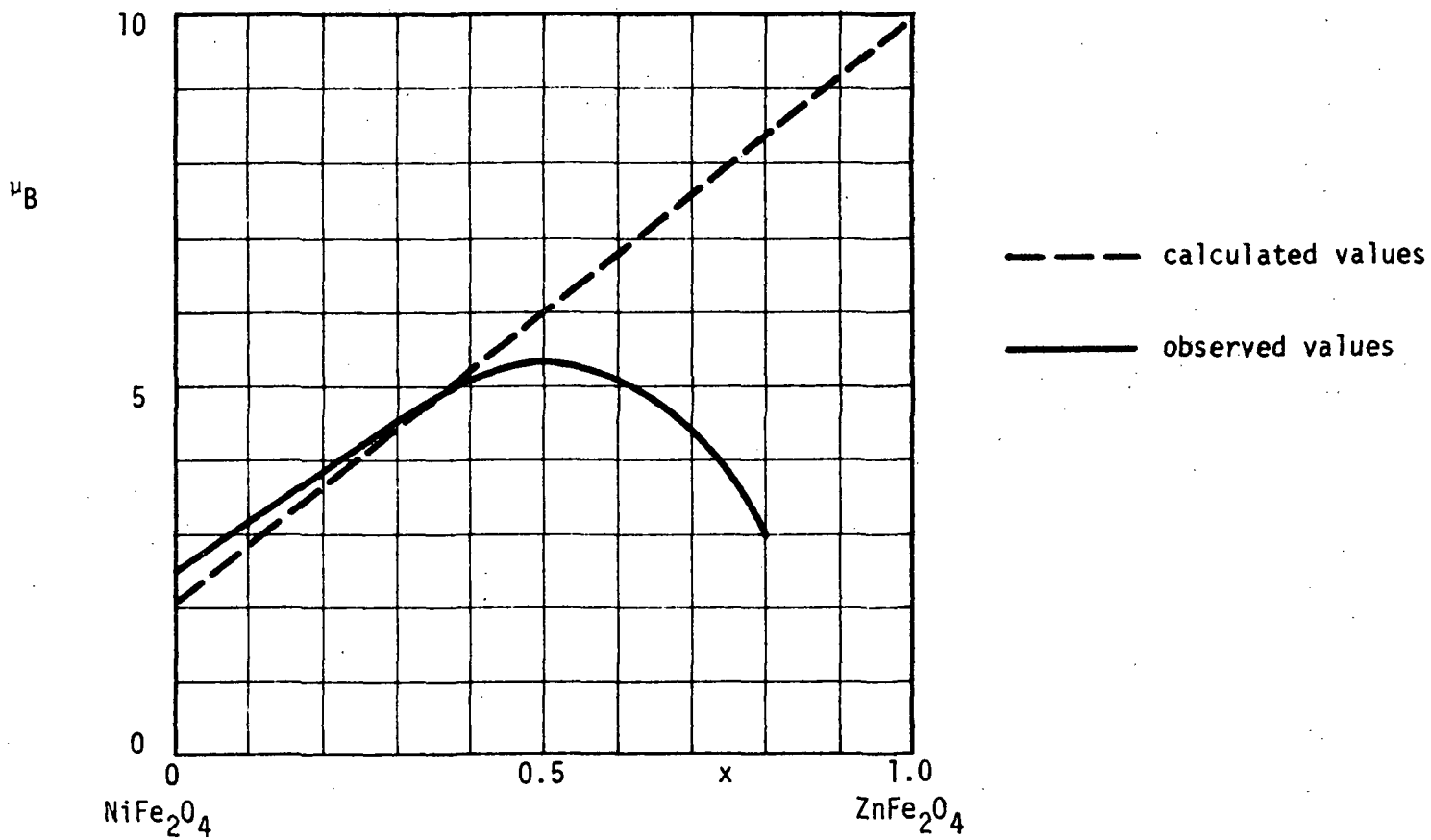

Figure I-4 Dependence of saturation moment per molecule for Ni-Zn ferrite on concentration of substituted zinc ions

4. Initial Permeability

A useful application of ferrites utilizes the linear B-H relationship at low flux densities which is related to the initial permeability, μ_i. The initial permeability may be defined as[22]

$$\mu_i = \frac{dB}{dH}\Big|_{H \to 0}$$

where B and H are physical quantities introduced previously. A high initial permeability produces large changes in flux density for small swings of the field intensity. Consequently, a larger inductance per turn can be realized resulting in increased efficiency of the ferrite core. Or, on the other hand, a smaller core may be fabricated yielding a comparable device as a larger core of different material with a lower μ_i.

It is generally believed that two factors contribute to the initial permeability of ferrites. One factor is domain wall movement, which is a displacement of the magnetic domain walls within the material. As a result, there is an increase in the volume of the domain that has its magnetization parallel to the applied field[23]. The other magnetization process is rotation of magnetic vectors of the domain (domain rotation).

It has not been decided which process contributes most to the initial permeability of sintered ferrites. Wijn and Went[24] concluded that after demagnetization in an a.c. field of decreasing amplitude, the magnetization of these materials is almost exclusively caused by spin rotation. Mechanical shock experiments to nickel-zinc ferrite specimens by Rathenau and Fast[25] support this conclusion. Guillaud[26] investigated the dependence of the initial permeability of manganese-zinc ferrites on grain size. He infers from this data that the permeability is due to a rotational process for grain size less than about 5μ in diameter and wall displacement for

grains between 5 and 20μ. Above 20μ the grains become porous and the permeability begins to decrease. On the other hand, Galt[27] has shown that in single crystal magnetite the high initial permeability is a result mainly of domain wall movement.

The initial permeability that arises as a result of rotations is proportional to

$$\frac{M_s^2}{K}$$

where M_s is the saturation magnetization and K is the magnetic anisotropy energy. The saturation magnetization is temperature dependent and is determined by a numerical solution of the Brillouin function. The anisotropy energy is related to a second or higher order of the spontaneous magnetization[28]. This results in a fairly complicated temperature dependence of initial permeability. Generally, the permeability increases up to a point and falls abruptly at the Curie temperature. It will be shown in Chapter IV that this discontinuity can be utilized for temperature detection.

II. MATERIALS PREPARATION

A. Mn_5Ge_3

Powders of electrolytic manganese (99.9%) and germanium (six nine purity) were mixed in the desired proportions and placed in a graphite crucible. The crucible is tapered to facilitate removal of the sample. Tantalum or vicor tubing could not be used to contain the specimen because of their reaction with the manganese. All compounds were prepared by melting the elements in the crucible under 2/3 atmosphere of argon in an induction furnace at 1300°C.

The high temperature reaction was accomplished with a Lepel rf generator with a maximum power output of 20 kw operating at 475KHz capable of temperatures up to 2000°C. A water cooled copper coil encloses the sample and induces eddy current losses or joule heating in the sample. The basic procedure using this generator is as follows:

1. Turn-on Procedure.

   The filament is turned on and 15 minutes is allowed for warm up prior to turning the plate on. Evacuation of the bell jar can be accomplished during this waiting period.

2. Atmosphere.

   The specimen is placed inside the rf coil and the bell jar is placed in position. The bell jar is evacuated to 15 microns pressure and flushed with argon and evacuated once more to 15 microns. The flushing procedure is repeated to insure an oxygen free environment for the reaction. Next, the bell jar is filled with argon to about 2/3 atmosphere. The partial pressure eliminates the sublimination of the manganese.

3. Heating

The power output of the rf generator can be accurately controlled in small increments with the precision controller. A rough control is possible by limiting the total output to 25%, 50%, 75% and 100%. Further control is possible with 0.1% incremental changes within the desired range of output power with a numerical readout from 1 to 1000. The limit is set to 50% of maximum output power and the dial readout is increased in steps of 50 every ten minutes from the starting point of 150 until the desired temperature is reached. Temperature may be monitored with an optical pyrometer. With the graphite crucible used in our experiment, 700 on the dial corresponds to 1300°C. The specimen is held at this temperature for 15 minutes then homogenized below the melting point of Mn_5Ge_3 (932°C) at 900°C for 1 hour. The corresponding setting for 900°C is 475. The specimen is allowed to cool in the inert atmosphere for three hours to prevent oxidation.

The material is ground with a mortar and pestle and sifted through No. 230 mesh (63 microns). A small amount is retained for x-ray analysis. An organic binder such as paraffin dissolved in benezene or butvar and acetone is added. The binder serves not only as a particle adherent, but as an insulator. The binder separates the particles and decreases the conductivity of the specimen. The powder with binder is pressed in a die at 5000 psi for five minutes. The final shape is cylindrical with 0.315 inches diameter and an average length of 0.350 inches.

Several attempts to alter the Curie point of Mn_5Ge_3 involved the substitution of various metals into the compound. The main criterion was atomic radius. Aluminum, gallium, iron, magnesium, vanadium and zinc were substituted for manganese while tin and silicon were used to replace part

of the germanium. Samples of each substitution attempt were examined with a General Electric x-ray diffractometer (Model No. XRD6) to determine the crystal structure. Of these metals, only iron yielded a homogeneous single phase material with the desired change in magnetic properties (see Chapter III). It was obvious from the x-ray data or by visual examination that the balance of elements did not enter the crystal structure.

Attempts to prepare the germanides by arc melting were unsuccessful. Briefly, this method consists of passing a high current arc through the sample which heats it to about 2000°C. The power supply is a dc welding generator (Model No. A4000HD-2A-SIL) manufactured by A.O. Smith and Company, capable of generating up to 400 amps. A cabinet made by NRC contains the melting chamber and vacuum equipment. The arc producing elements are a non-consumable tungsten electrode and a water cooled copper hearth which serves as the anode. The materials to be melted are placed on the copper hearth which is then bolted to the bottom of the chamber forming a vacuum tight seal. An inert atmosphere is prepared similar to that mentioned above. For our experiment, we passed 70 amps through the material for approximately 10 seconds. It is extremely difficult to prevent the arc from scattering the materials thus destroying the starting composition. As a result, this method was abandoned, and the germanides were prepared with the aid of the induction furnace.

B. FERRITES

The formation of polycrystalline ferrites is usually accomplished by some type of solid state reaction. For example, $Ni_{0.3}Zn_{0.7}Fe_2O_4$ is a result of the reaction

$$3NiO + 7ZnO + 10Fe_2O_3 \rightarrow 10Ni_{0.3}Zn_{0.7}Fe_2O_4$$

The oxides must be mixed intimately and heated to at least 1200°C. This temperature is referred to as the sintering temperature and is performed at 50 to 100°C below the melting point of the ferrite. The addition of zinc lowers the melting point of most ferrites, thereby lowering the firing temperature. If samples of $Ni_{1-x}Zn_xFe_2O_4$ are fired at the same temperature with various values of x, the one with the highest zinc content will have the greatest density. The resulting ferrite has a hard, black, non-porous ceramic appearance.

The preparation of ferrites requires a great deal of art due to the many variables encountered in the process. At present, the parameters such as firing time, temperature, atmosphere and exact composition are determined by repeated experimentation in order to produce ferrites with the desired characteristics. For example, the firing temperature, time and atmosphere have a profound effect on material properties. The valence state of the metal ions present (Fe^{2+}, Fe^{3+}) depends on the amount of oxygen taken into the lattice and may vary with temperature and partial pressure of oxygen during sintering thereby affecting the electrical and magnetic properties of the solid.

1. General Process

There are four basic steps in ferrite preparation:

(1) mixing;

(2) prefiring;

(3) powdering and pressing into final shape;

(4) sintering.

The prefiring and powdering steps may be repeated to obtain a high degree of homogenuity. The entire preparation process is illustrated in Figure II-1.

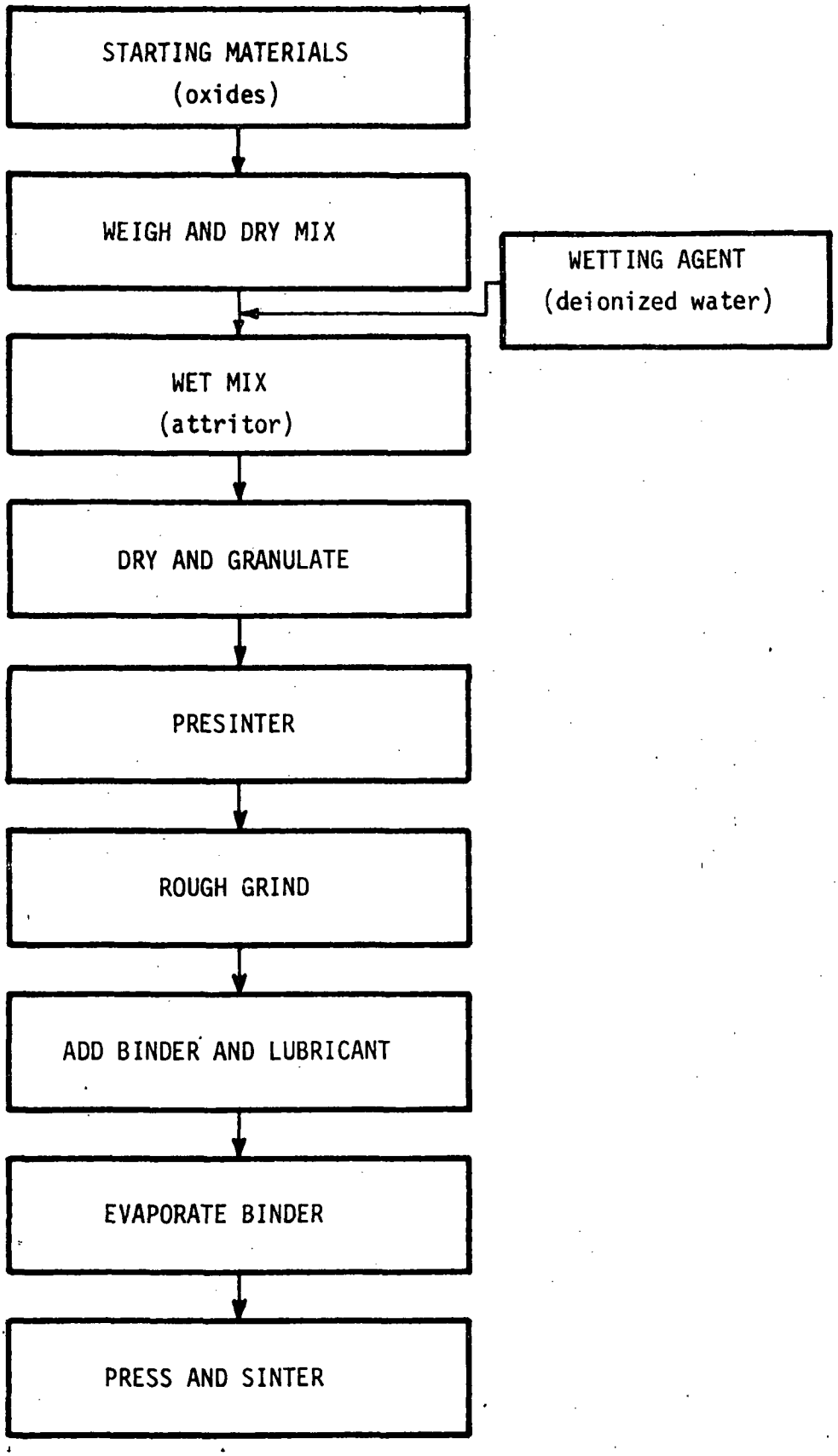

Figure II-1 Fabrication process for ferrites

Of several methods of mixing reported, three will be mentioned here. The oxide method involves the wet milling of high purity oxides in the correct proportions. This is discussed in depth below. Decomposition methods differ from the oxide method only in the fact that salts, such as carbonates, nitrates and oxalates are mixed (milled). The material is then heated to produce the oxides by decomposition. As the chemical bond is broken, carbon dioxide is given off leaving the metals in their nascent state. At this stage, the metals are more active. As a result, this method produces materials which more readily undergo solid state reaction at a lower temperature.

The third method offers the advantage of creating an intimate mixture without mechanical mixing. This involves the co-precipitation of the hydroxides or oxalates from mixed solutions. It should be noted that the chemical processes must be thoroughly understood to insure complete and simultaneous precipitation. Knowledge of the soluability products are essential to determine the pH for complete precipitation. If simultaneous precipitation is not achieved, the value of the method is lost. Removal of the precipitation agent and/or filtration or decantation of the ions may present difficulty with the hydroxide method. As a result, preparation of the oxalates may be preferable because precipitation may be carried out with ammonium oxalate which leaves no residue after ignition. Also, most of the oxalates are very similar in crystal structure. Therefore, mixed crystals can be produced which contain the metallic cations in the original proportions.

To avoid lengthy milling time and inadequate mixing, the precipitation methods were first attempted. Nickel, iron, and zinc in the correct proportions were dissolved in nitric acid (HNO_3) with ammonium hydroxide

(NH_4OH) as the precipitating agent. Individual precipitation of the hydroxides and electron probe analysis revealed the absence of zinc. Two reasons may be cited for incomplete precipitation of the zinc ions. Zinc forms a very stable complex ion with ammonium ($Zn(NH_3)_4^{++}$) which is soluble in H_2O. Secondly, the addition of more alkali (NH_4OH) results in the following reaction:

$$Zn + OH^- + H_2O = HZnO_2^- + H_2$$

which may go to

$$ZnO_2^= + H_2O$$

The complex ion $ZnO_2^=$ is also soluble in H_2O. Peroxides in alkaline solution form with zinc salts the hydrated zinc peroxide, $ZnO_2 \cdot 2H_2O$[29,30].

An alternate method utilizes oxalic acid and ammonium oxalate as precipitating agents. Due to different ionic states or iron, neither would yield complete precipitation of iron oxalate (FeC_2O_4). Since all the ions were not precipitated simultaneously, the method was lost.

2. Mixing

The ferrites presented in this paper are a result of the mechanical mixing of the oxides. The mixing is performed with a Research Model Attritor #01 from Union Process, Inc. Use of the attritor results in a dispersion approximately 80 times faster than conventional milling techniques. The attritor consists of a stainless steel grinding tank with a capacity of 400 cc and a variable speed agitator arm. The stationary tank is jacketed and permits temperature control; therefore, grinding can be performed at a predetermined temperature, hot or cold. Cooling is accomplished by circulating tap water through the jacket. The grinding elements are 5 mm diameter carbon steel balls and the wetting agent is deionized water.

The grinding process can be checked any time during the run, and the dispersive action can be observed with a microscope.

The starting materials are Fe_2O_3, NiO, and ZnO powders. The Fe_2O_3 and NiO are processed by Baker Chemicals and are 99.7% pure. The ZnO powder is produced by Baker and Adams and is 99.0% pure. The importance of purity in the starting materials cannot be overemphasized. The impurities present may alter the stoichiometry or worse yet, participate in the reaction with undesired results. An analytical balance with an accuracy of 0.0001 gram is used to measure the correct proportions of oxide.

(a) Mixing Speed.

The average sample weight is 130 grams. The oxides are dry mixed by hand obtaining a homogeneous color and placed in the attritor tank. Approximately 800 grams of carbon steel balls and 275 cc of deionized water was added. The preferred rpm of the agitating shaft is between 250 and 360[31]. It was desirable to avoid splatter of the mixture on the tank cover and still achieve an intimate mixture in a reasonable amount of time. Therefore, the maximum operating speed of the shaft was 300 rpm.

(b) Mixing Time.

Both the transition temperature and permeability are composition dependent; hence, it is important to control the introduction of impurities. Assuming sufficiently pure starting materials, the main place contamination occurs is in the mixing procedure. Obviously, an effective grinding and mechanical dispersion of the oxides cannot be accomplished without some contribution of foreign material from the grinding elements. In this case, the steel balls, agitating arm and grinding tank of the attritor assembly were in vigorous contact with the starting materials. A balance must be obtained with the mixing time such that an acceptable dispersion is

accomplished with a minimum of contamination. With this in mind, a series of experiments were performed to determine the optimum mixing time. The sharpest transition was the desired results. Samples of the mixture were removed at specific intervals and sintered at the same temperature. Figure II-2 illustrates the initial permeability versus temperature curves of $Ni_{0.264}Zn_{0.736}Fe_{1.95}O_4$ for various mixing times. The optimum mixing time was chosen to be three hours with a mixing speed of 300 rpm.

In order to determine the amount and type of impurities picked up during the mixing process, we analyzed the residue from the attritor. The attritor was cleaned thoroughly and filled with distilled water and about 800 grams of the steel balls. The mixer was operated at the normal mixing speed of 300 rpm for three hours. The water was separated from the balls and placed in a beaker and the impurities were allowed to settle out. Approximately 1/2 gram of a metallic appearing powder was obtained and was analyzed with a Phillips Electron Probe Analyzer (Model No. AMR/3). The powder was mostly iron with small amounts of nickel and zinc. This indicates that the attritor was not cleaned properly from the prior mixing or that a considerable amount of iron was picked up from the grinding elements. This amount of contamination, however, only amounts to less than 0.4% of the total sample weight.

Discharging of the finished dispersion is accomplished by removing the grinding tank from the assembly. The contents are discharged through a 16 mesh screen which allows the dispersion through and retains the grinding elements. The mixture is dried in a Pyrex beaker at 120°C.

Prefiring the oxides may play an important role if a high degree of homogenuity and a minimum of shrinkage in the final form is desired. Several samples were prefired at various temperatures and times. X-ray

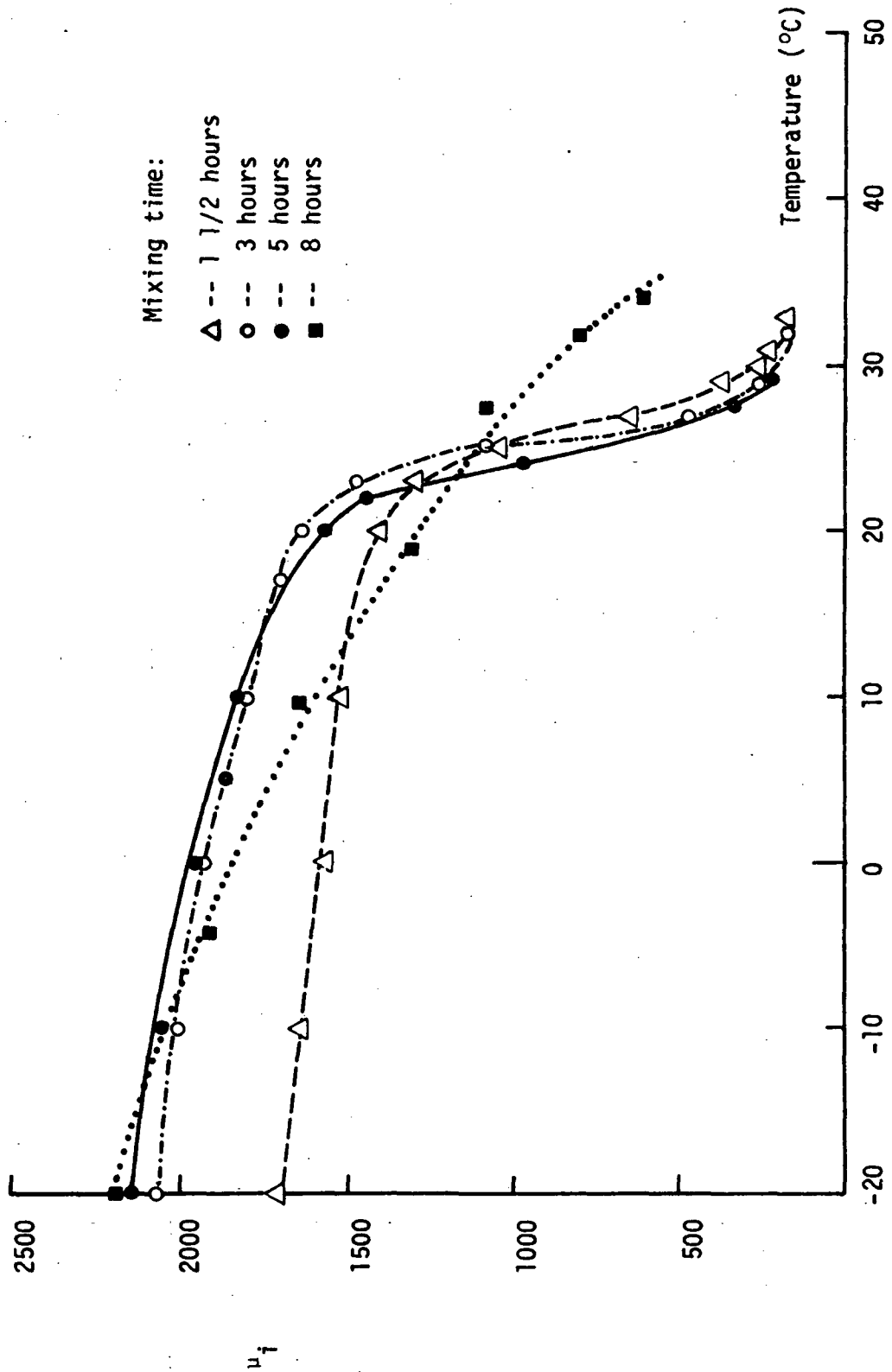

Figure II-2 $Ni_{0.264}Zn_{0.736}Fe_{1.95}O_4$. Initial permeability versus temperature for various mixing times

analysis revealed the formation of the spinel structure at 700 C and excess nickel and iron oxides. This indicates that zinc ferrite forms during prefiring. We sintered samples to determine the effects of prefiring on the transition. It was decided that the prefiring step is unnecessary for this composition.

3. Pressing

The final shape of the sample is toroidal and is chosen to simplify permeability calculations (see Appendix A). The dried oxides are mixed with an organic binder consisting of Butvar (a polyvinyl butyral resin) dissolved in acetone (CH_3COCH_3). A solution of 0.5 grams Butvar is dissolved in 100 cc of acetone. 0.7 cc of solution is added per one gram of oxides and allowed to dry. The appropriate die is shown in Figure II-3, and is used with a Carver Laboratory No. 14600-15 hydraulic press. One gram of the powder with binder is placed in the die and a pressure of 6000 psi is maintained for two minutes. An organic binder, such as mentioned above, facilitates an intimate contact of the oxides. With sufficient pressure, the binder becomes liquid and lubricates the powder allowing a denser shape. This decreases the fragility of the sample and aids the solid state reaction.

4. Sintering

The toroids are placed on a boat covered with platinum foil and then in a furnace for the high temperature reaction. The toroids had a tendency to adhere to substances such as ceramics or firebrick, thus necessitating the use of platinum foil. The furnace is a horizontal Lindberg Hevi-Duty glow bar type furnace with a maximum temperature of 1500°C. Figure II-4 shows the heating and cooling schedule. Decomposition of the binder is performed at 300°C for 30 minutes. The volatilization of the binder must occur slowly or cracking of the toroid will result. The samples are heated

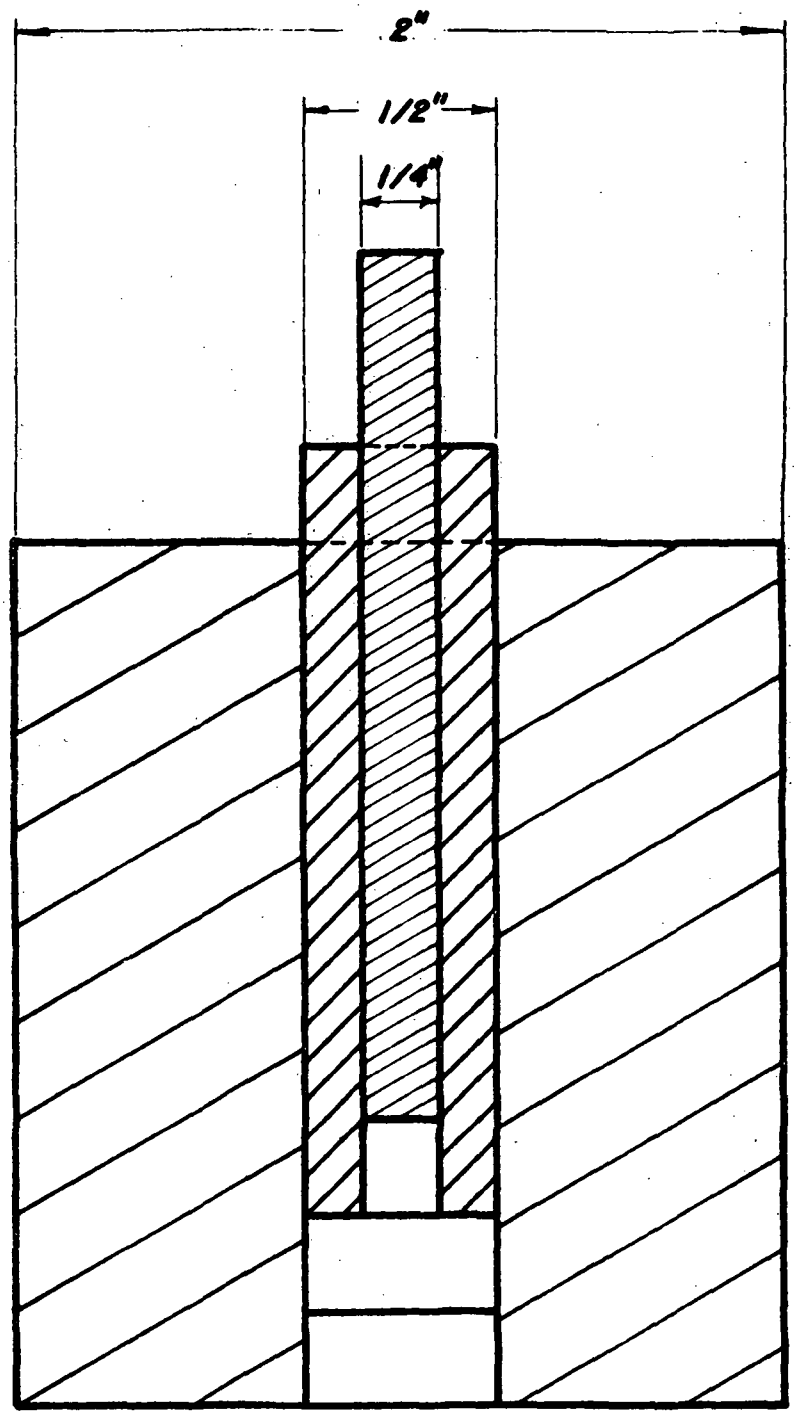

Figure II-3 Toroidal die

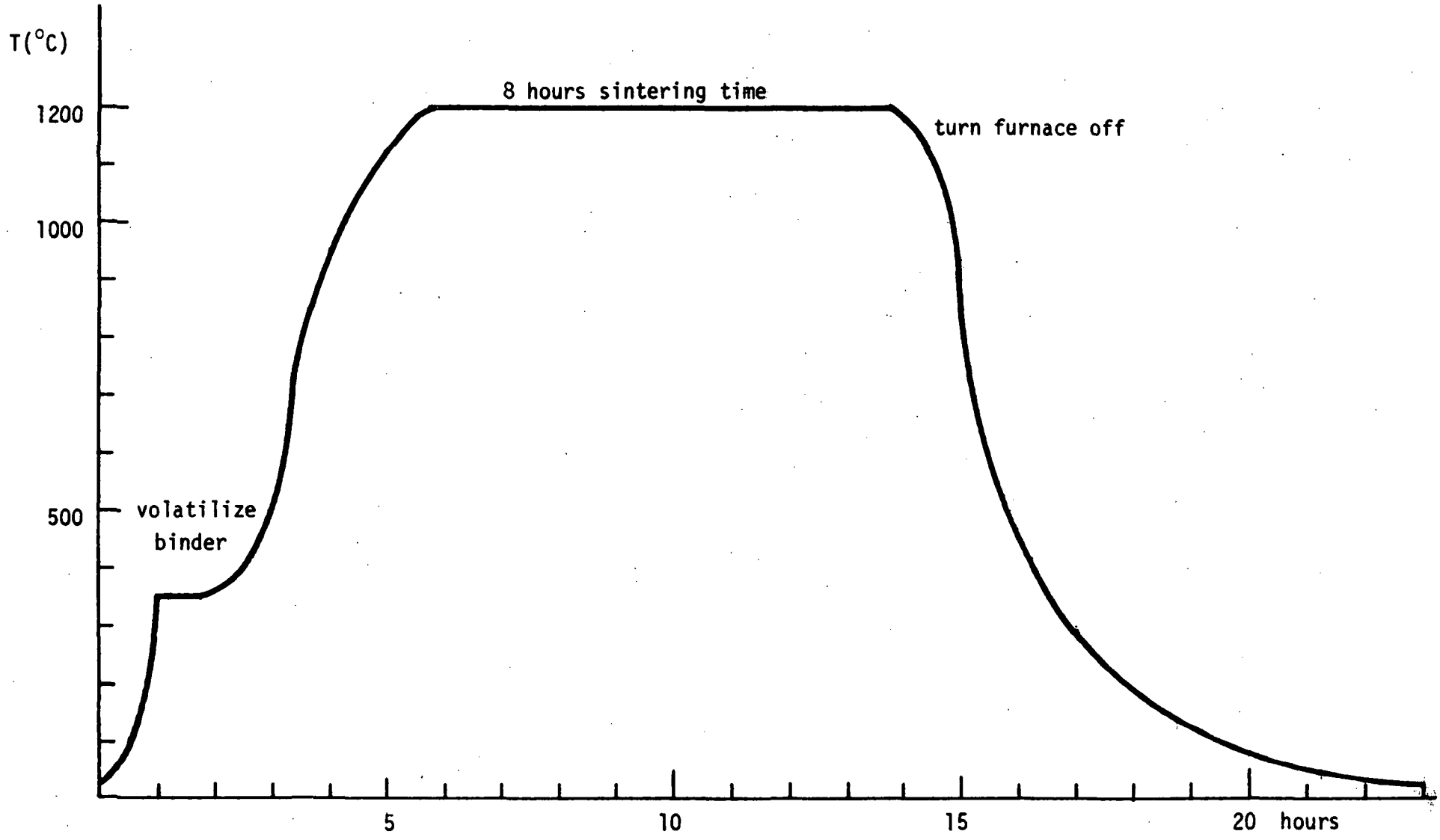

Figure II-4 Heating schedule for ferrite preparation

in the furnace to 1200°C in air. This temperature is maintained for 8 hours and the power to the furnace is shut off. A word is in order concerning the temperature calibration with this furnace. The controller operates from the output of a thermocouple. This thermocouple can be placed inside the furnace tube (at the flat zone) or from the side adjacent to the tube. It was necessary to place the thermocouple from the side to provide maximum space inside the furnace. At 1200°C, we found a difference of 30°C between the two positions. Therefore, we set the controller at 1230°C for operation at 1200°C.

Alternate heating methods were tested and their effects are shown in Figures II-5,6,7. After the binder was volatized, the samples were placed directly into a preheated furnace at various temperatures. This is referred to as fast heating. Slow heating refers to the schedule in Figure II-4. Once the heating rate and temperature was chosen, the sintering time was varied. Figure II-7 illustrates the transitions of various samples of $Ni_{0.28}Zn_{0.72}Fe_{1.95}O_4$ fired at 1200°C as a function of firing time. It is clear that the sample fired for 8 hours has the sharpest transition.

As stated in Chapter I, the transition temperature of nickel-zinc ferrite is a function of composition. Figure II-8 shows the Curie point of $Ni_{1-x}Zn_xFe_2O_4$ as x is changed. The accuracy of the starting composition is limited by the analytical balance and is approximately one part in 10^6. This corresponds to an accuracy of approximately 0.1°C. However, we realized an accuracy of 5°C experimentally.

5. Alteration of Stoichiometry

The complex ions of nickel and zinc can be added in liquid form allowing much more accurate control of composition changes (1 part in 10^8). In addition, the composition can be altered without repeating the entire mixing process. Nickel acetate ($Ni(C_2H_3O_2)_2 \cdot 4H_2O$) and zinc acetate

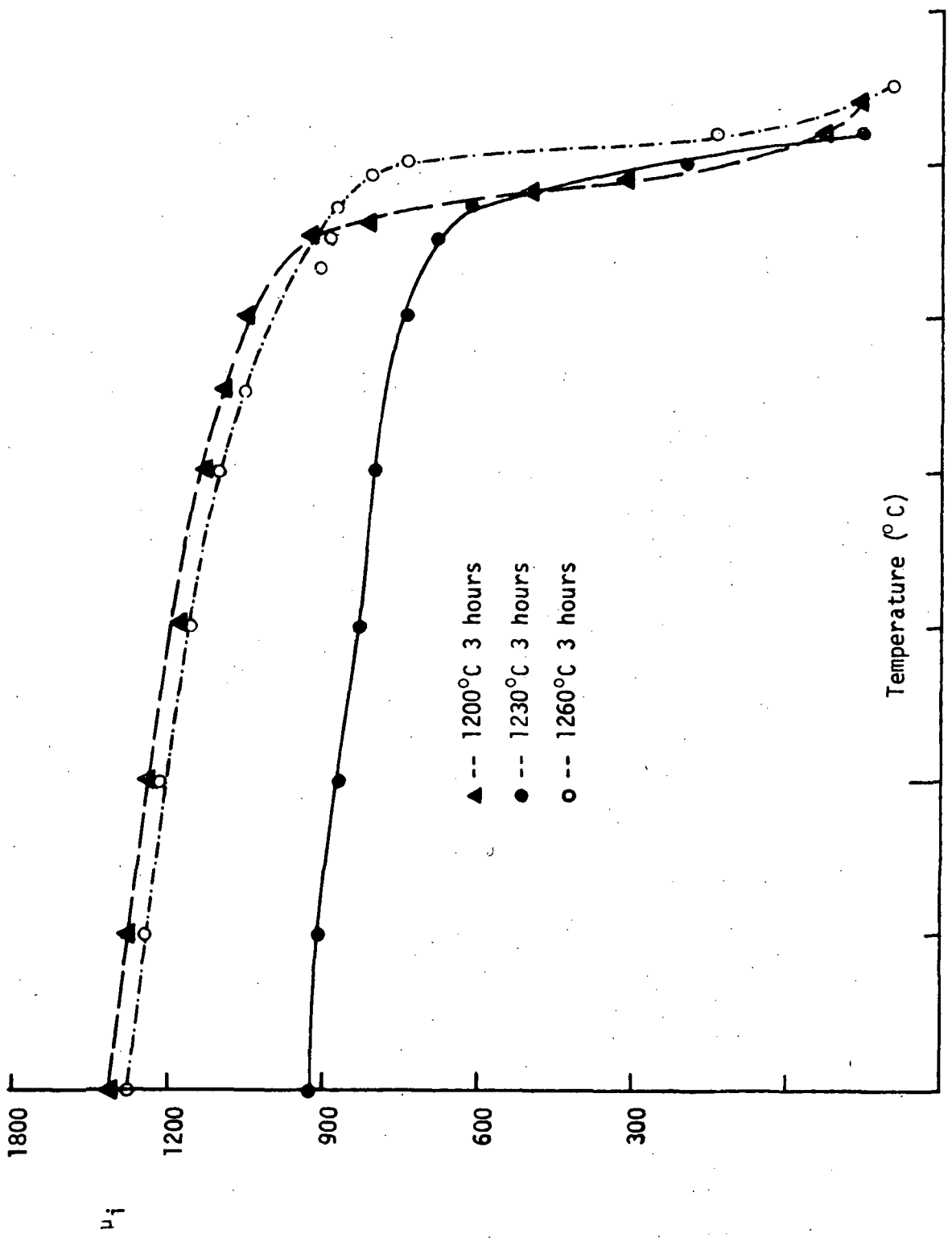

Figure II-5 $Ni_{0.28}Zn_{0.72}Fe_{1.95}O_4$ Slow heating to sintering temperature

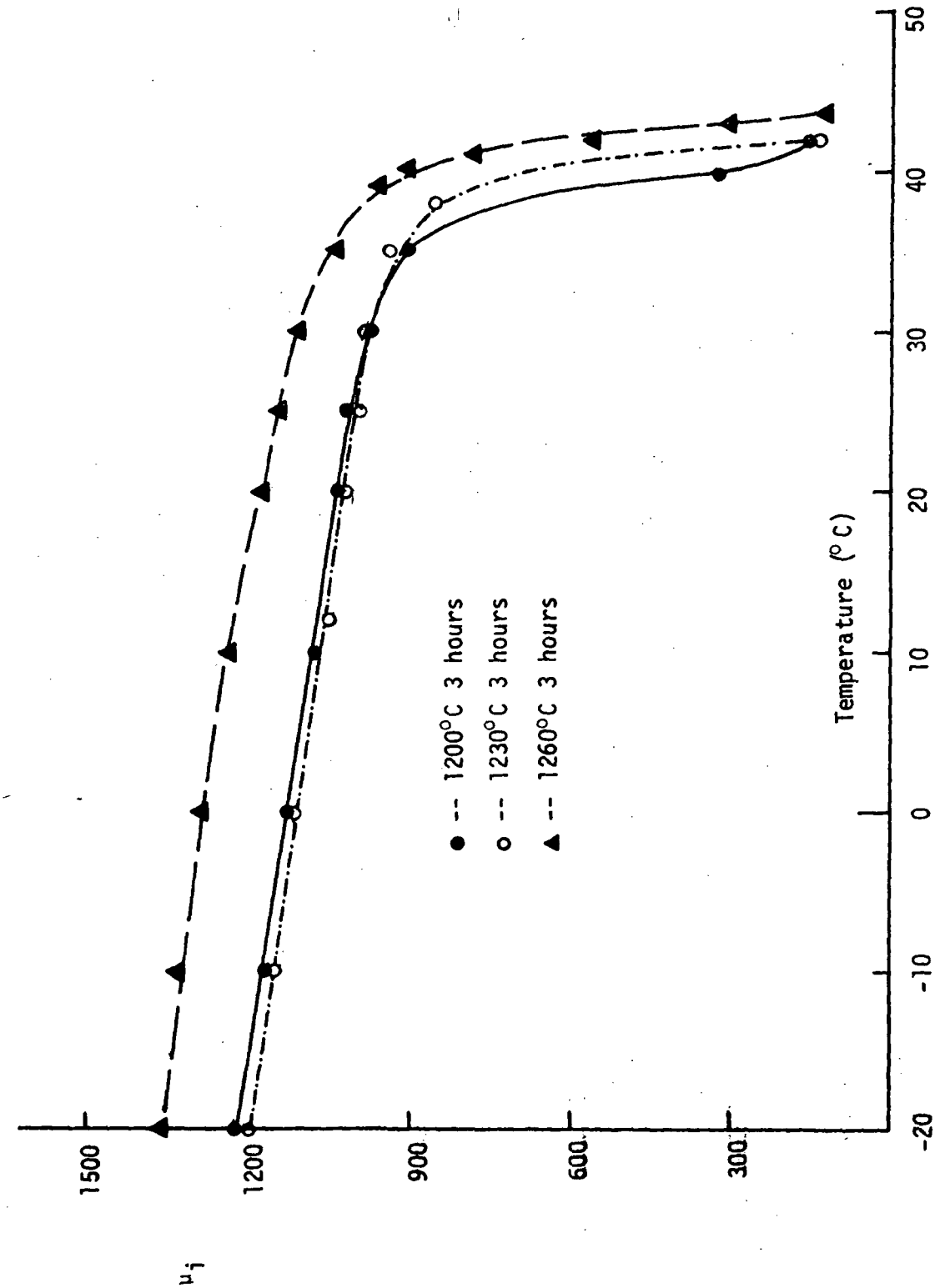

Figure II-6 $Ni_{0.28}Zn_{0.72}Fe_{1.95}O_4$ Fast heating to sintering temperature

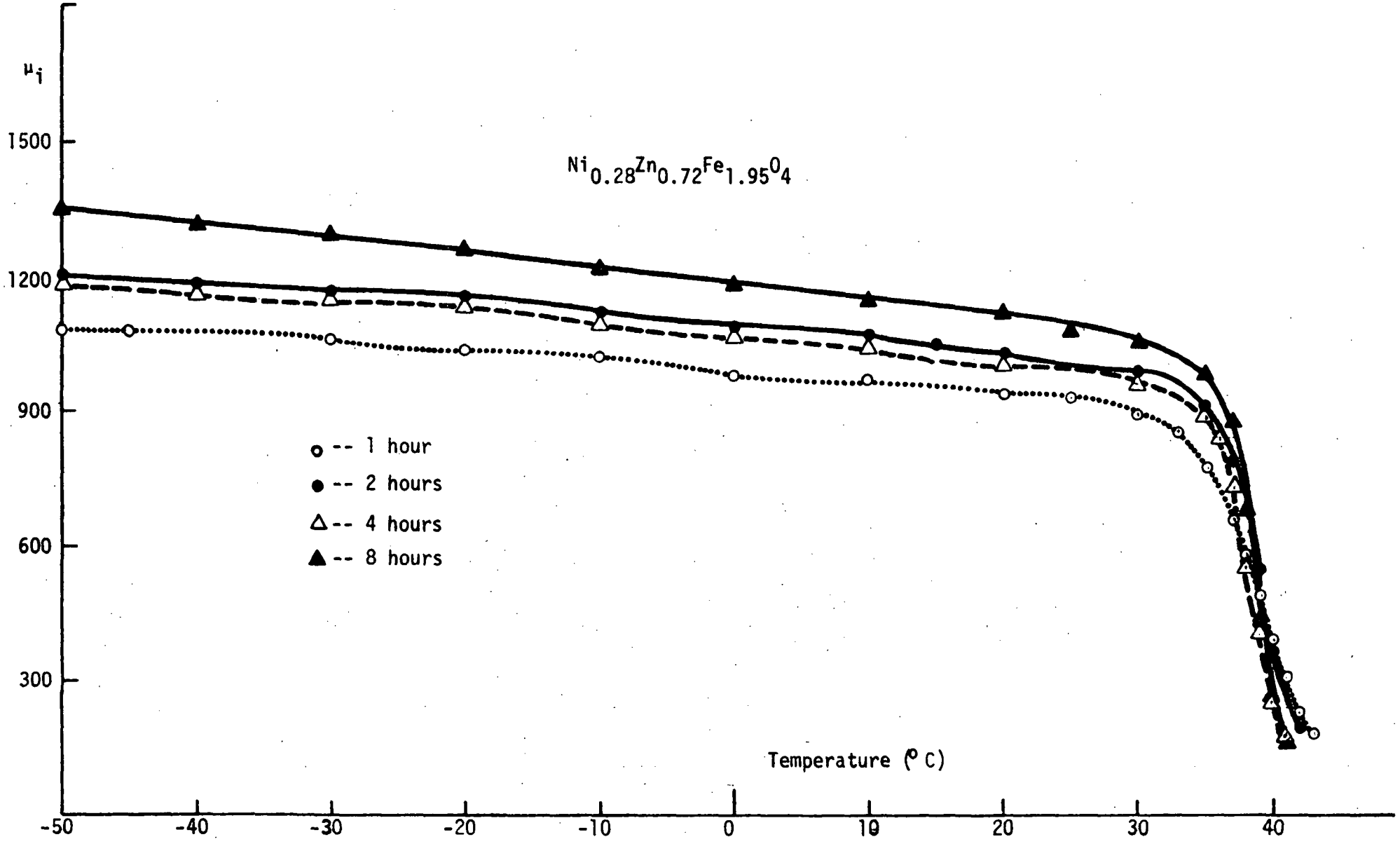

Figure II-7 Sintering time

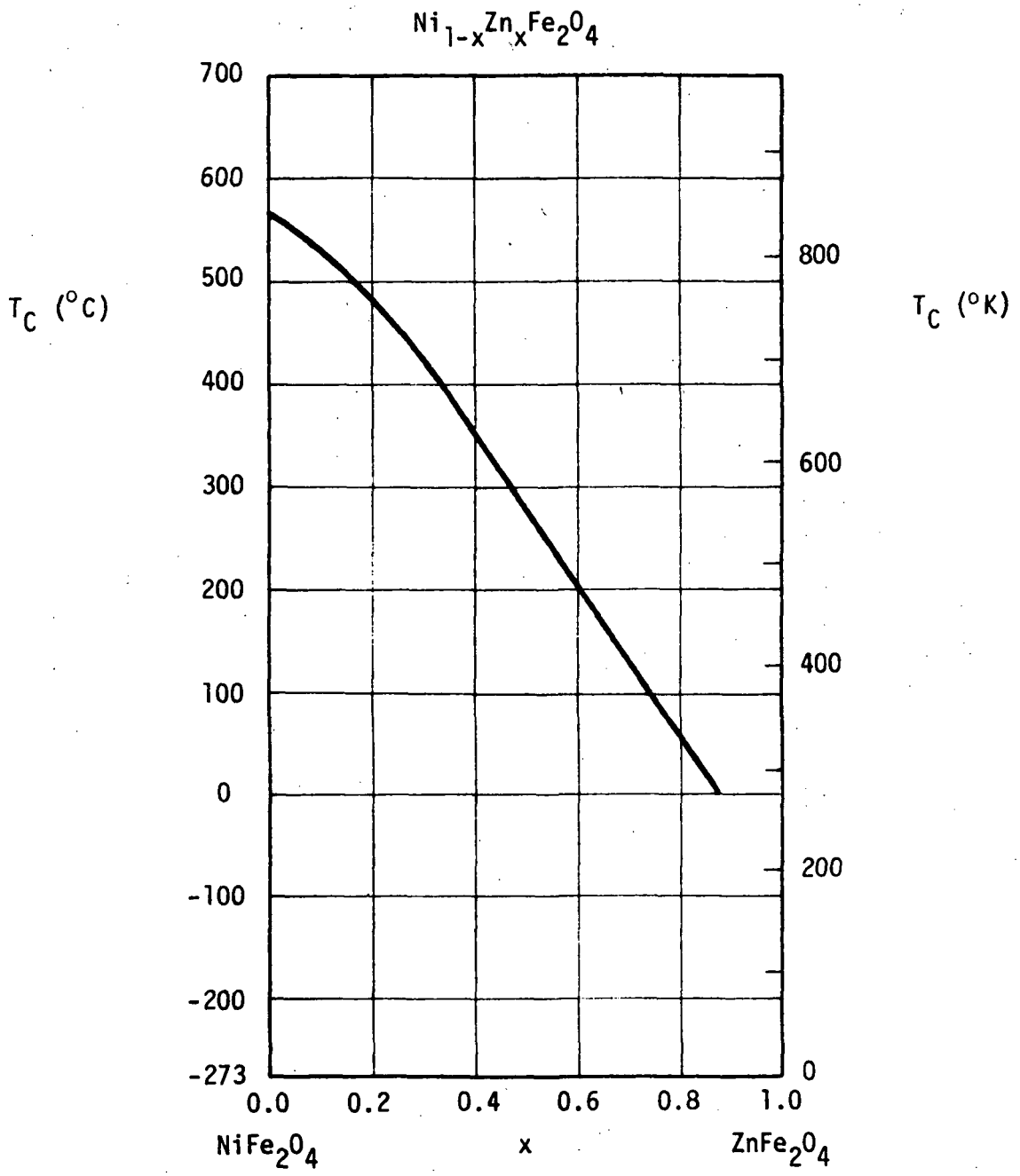

Figure II-8 Curie temperature (T_C) of Ni-Zn ferrite as a function of the zinc concentration. (After Smit and Wijn[32])

($Zn(C_2H_3O_2)_2 \cdot 2H_2O$) readily dissolve in water and decompose to nickel oxide and zinc oxide, respectively, at 200 to 300°C as validated by x-ray diffraction experiments. 0.7 cc of varying concentrations of the acetate solution is used to wet one gram of the oxide powders. As shown in Chapter III, the addition of nickel acetate shifts the transition temperature higher as expected. Conversely, we expected the Curie temperature to be lowered with zinc acetate additions. Several attempts were made to accomplish this, but were unsuccessful. We knew from preliminary experiments that the decomposition of zinc acetate yielded the correct amount of zinc oxide so no zinc losses were expected. We first added the acetate solution to the powders as above and then let it dry at room temperature. The powder is then pressed into a toroid and sintered. As a variation of this, the powder can be heated on a hot plate after the acetate solution is added and the acetate compound can be broken down prior to pressing and sintering. Neither of these methods yielded the desired results with zinc acetate. On the other hand, both methods were tried with the nickel acetate addition and again it made no difference if the acetate was decomposed prior to pressing and sintering. Figure II-9 illustrates the effects of the addition of zinc acetate. It can be seen that the major effect is only to lower the permeability.

6. Resistivity

Figure II-10 illustrates the abrupt changes in resistivity of nickel zinc ferrite that occur as the stoichiometry changes from an iron excess to an iron deficiency. Oxygen loss leads to the presence of Fe^{2+} ions in the lattice. High conductivity is contributed to the occurrence of both Fe^{2+} and Fe^{3+} upon identical (octahedral) lattice sites in the spinel structure. Electrons can transfer from the divalent ferrous ion at the B site to the trivalent ferric ion at the same site without causing a change in the energy

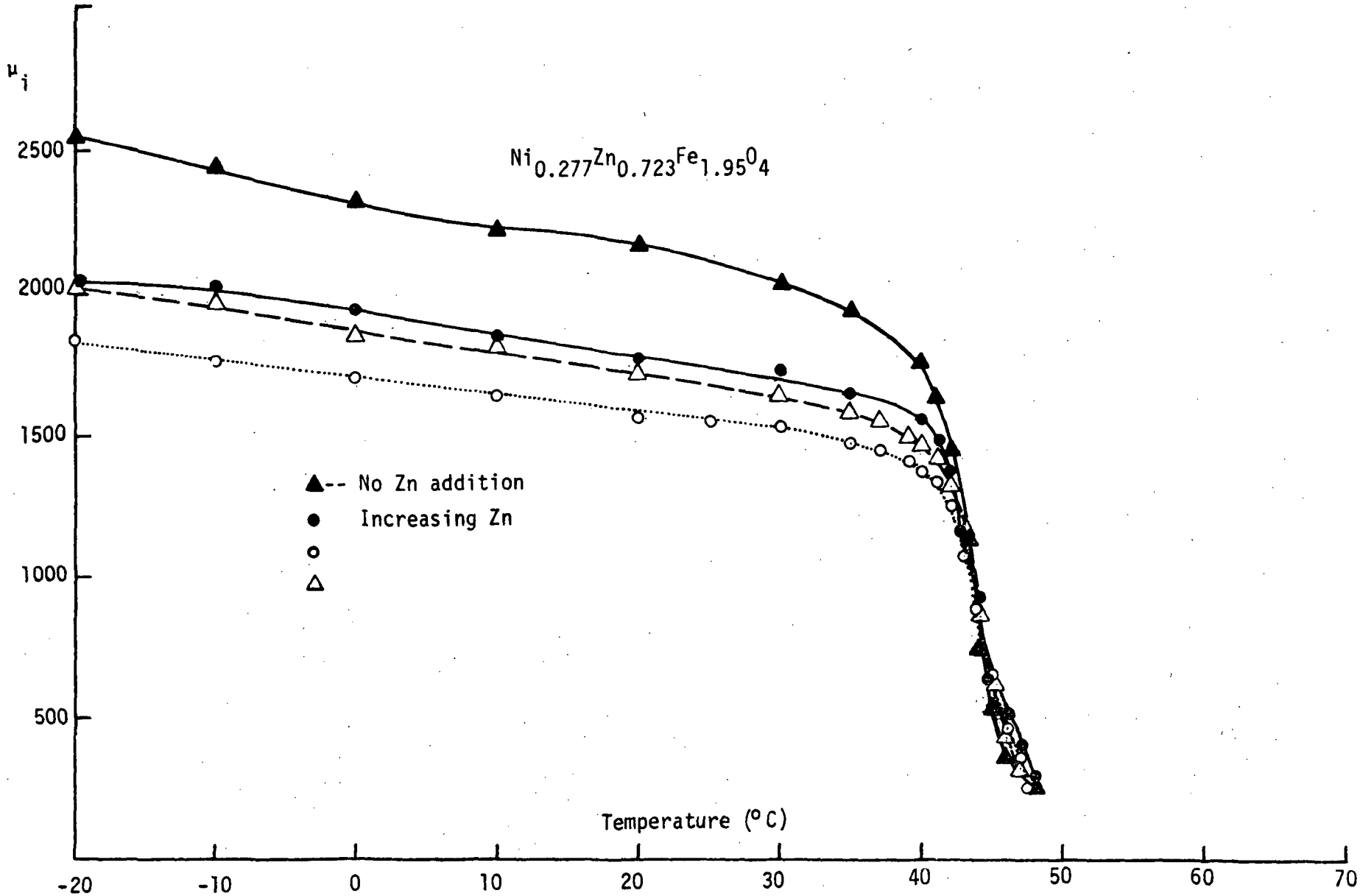

Figure II-9 Zinc doping

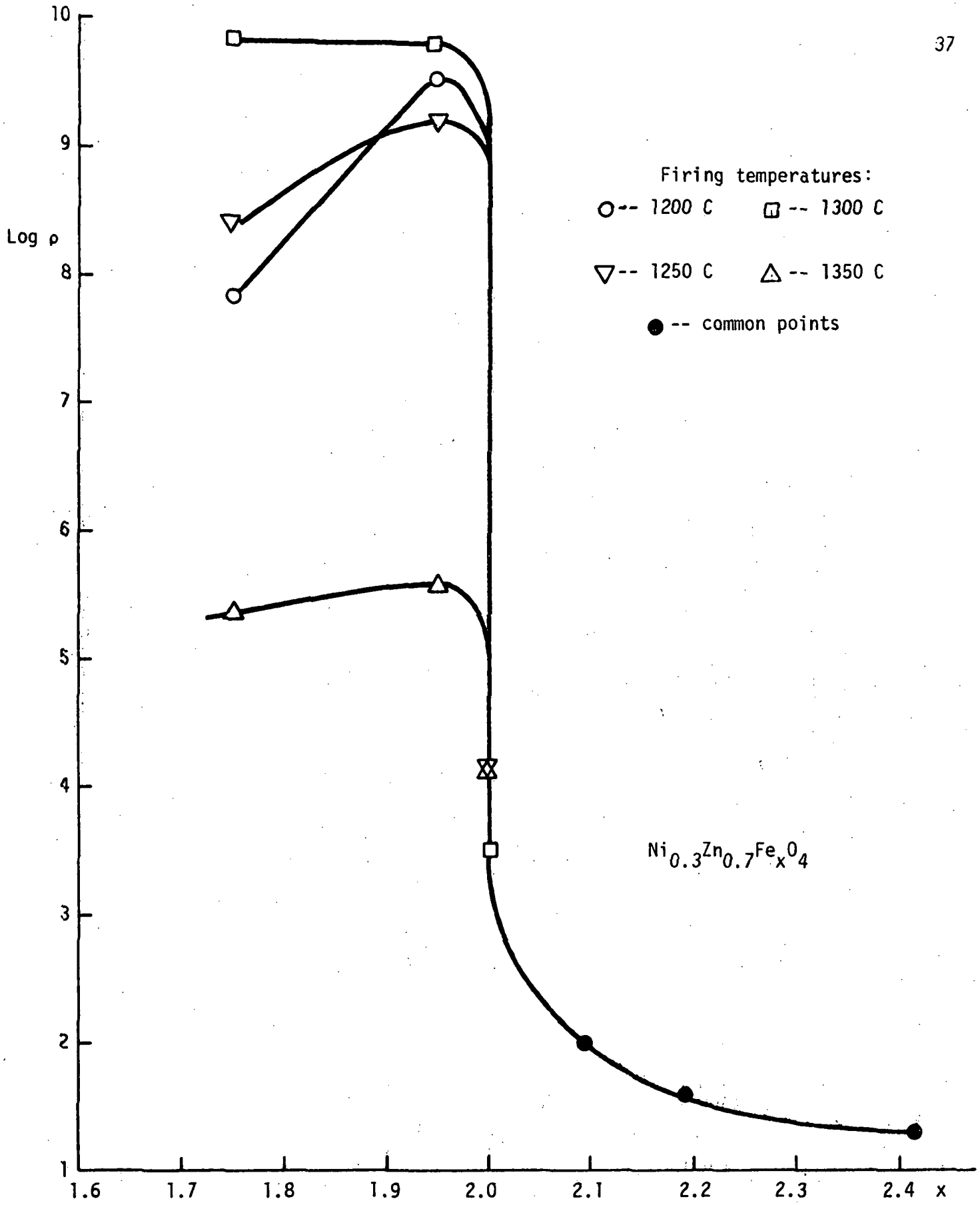

Figure II-10 The variations of resistivity with firing temperature and iron stoichiometry (After van Uitert 1955)

state of the crystal. Thus, it might be expected that electron flow would be facilitated, giving rise to high conductivity. It is important in many applications to control the resistivity of ferrites. Two general approaches have been made to this problem: (1) controlling the firing temperature and atmosphere; (2) addition of minor constituents to decrease or increase the conductivity. This paper will consider the latter method. The classic example is magnetite, Fe_3O_4, which has a resistivity of about 5×10^{-3} Ω cm at room temperature. However, if the ferrous ion is replaced by the divalent metallic ion M, or decreasing the iron content in Ni ferrite, it is now no longer possible for electrons to be interchanged between the Fe^{3+} and the Ni^{2+} at the B sites. The resistivity can be increased in this way to about 10^7 Ω cm. The starting composition of the ferrites presented in this paper was deliberately altered off stoichiometry (i.e., $Ni_{1-x}Zn_xFe_{1.95}O_4$) to achieve high resistivity.

III. DATA AND RESULTS

A. MEASUREMENT TECHNIQUE

The ferrite specimens were toroidal with an average outside diameter of 11.0 mm, inside diameter of 5.3 mm and 2.8 mm thick. The samples were wound with 50 turns of #28 enamel coated copper wire and the permeability was calculated as shown in Appendix I. Since the Mn_5Ge_3 samples were cylindrical, a solenoid was fabricated to receive the specimens. The inductance was monitored with a General Radio impedance bridge (Model No. GR1650) at 1 KHz signal frequency. The output of the bridge detector circuit was coupled with a 1 KHz tuned detector to eliminate harmonic effects and increase the accuracy of measurements.

It was necessary to measure the inductance of the samples over a wide range of temperatures and maintain sufficient accuracy to observe incremental changes near the transition temperature. This was accomplished with a Lauda/Brinkmann Circulator (Model No. K-2/R). This circulator is equipped with a solid state thyristor controlled system which operates a 1500 watt heater and a compressor/condensing system yielding an operating range from -70°C to +150°C. A rotating magnet thermoregulator (contact thermometer) permits a temperature control accuracy of 0.02 C. Distilled water is used as the bath in the temperature range from +1 C to 95°C. Below 1°C, a 50:50 isopropyl alcohol/water mixture is substituted.

B. EXPERIMENTAL RESULTS

1. Mn_5Ge_3

(a) Iron Substitution

The transition of Mn_5Ge_3 occurs between 35 and 40°C. We were able to shift this transition higher with the substitution of iron for the manganese. All attempts to lower the Curie temperature were unsuccessful. Figure III-1

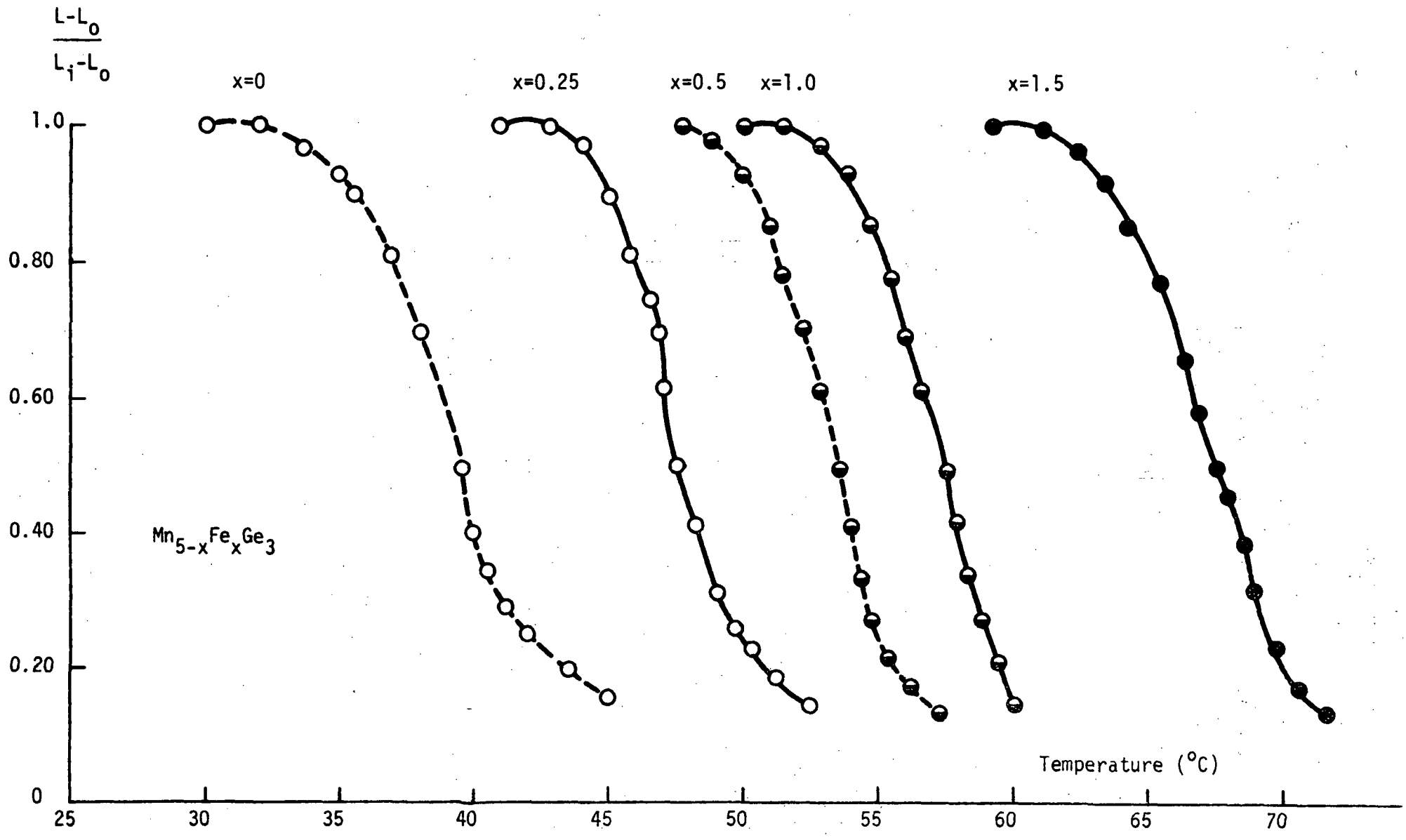

Figure III-I Normalized permeability versus temperature for iron substitutions

shows how the Curie point was altered with iron substitution. Here we show the transitions of $Mn_{5-x}Fe_xGe_3$ for x = 0, 0.25, 0.5, 1.0, and 1.5. The vertical scale is

$$\frac{L - L_o}{L_i - L_o}$$

where L is the measured inductance, L_o is the empty solenoid inductance and L_i is the value of inductance below the transition temperature. The inductance L_i is a maximum and is constant far below the transition. It is useful to define the transition temperature as the point where the inductance falls to 50% of the original value. With this criteria in mind, we show how this transition varies as a function of x in Figure III-2. The greatest change in transition temperature for iron addition occurs for $x < 0.5$. For $0.5 < x < 1.0$, the transition is less sensitive to extra iron. Finally, for $x > 1.0$, there appears to be an increasing sensitivity to additional iron. In conclusion, we were able to place the transition anywhere from 40°C to 67°C with a minimum of 1.0°C accuracy by controlling the starting composition.

We expected this material to be a permanent magnet with the c-axis being the easy axis. It turns out that it is a soft magnetic material with a low permeability possibly because of complicated spiral spin configurations. The spins are not parallel to the c-axis as predicted. In any case, the material is not a simple ferromagnetic material. The permeability was not measured directly, but it is estimated to be between 3 and 10.

2. Nickel-Zinc Ferrites

(a) Control of Transition Temperature

A much higher permeability (2000 to 4000) and wider range of transition temperatures are available with the nickel-zinc ferrite series. It was known from Figure 8 in Chapter II how the Curie temperature varied as

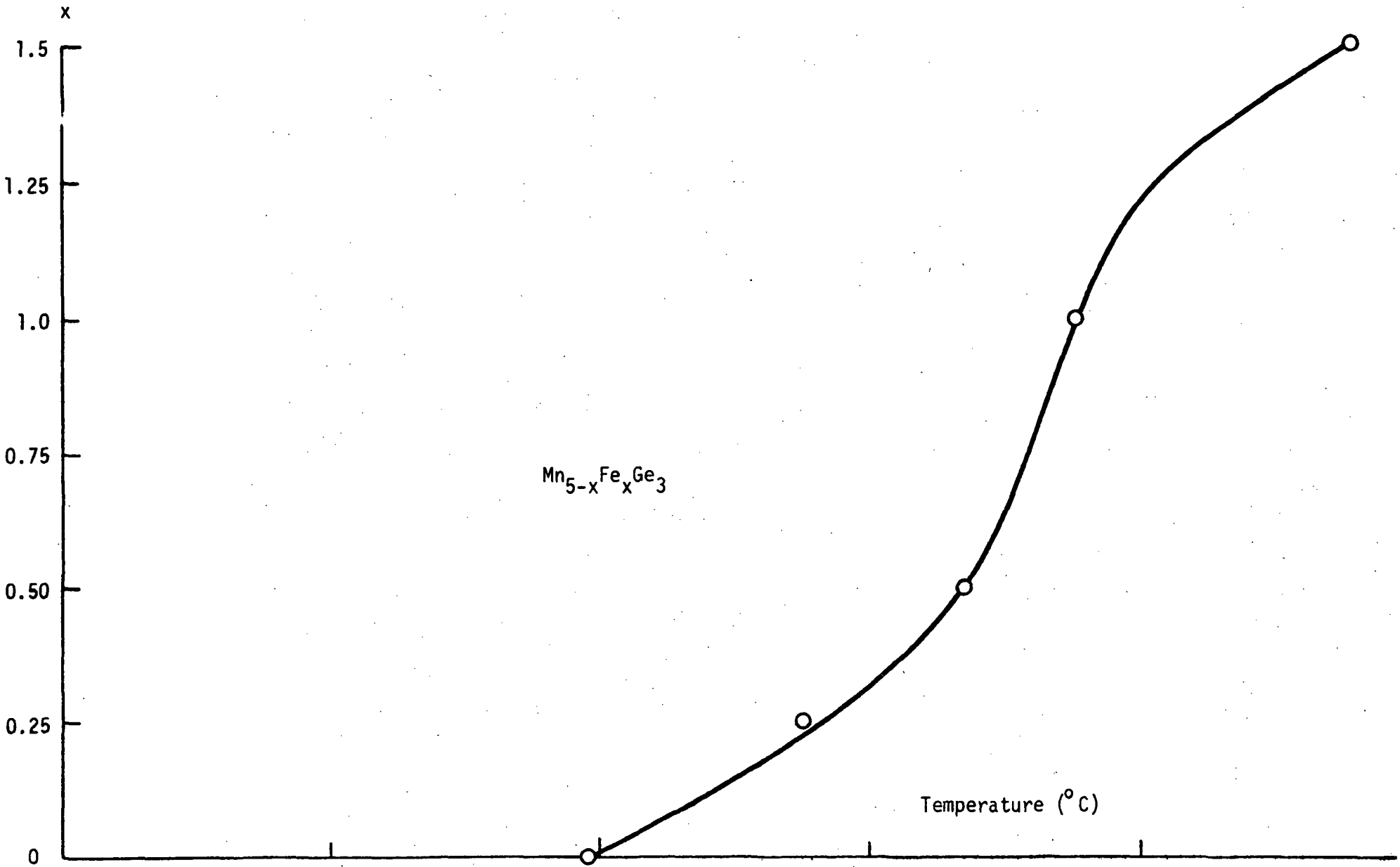

Figure III-2 Transition temperature versus iron substitution

a function of composition (nickel:zinc ratio). Careful replotting of this curve revealed the approximate composition necessary for a desired transition temperature. Control of the ratio of the starting materials allowed the setting of this transition with an accuracy of 5°C or less. Figure III-3 shows the normalized permeability versus temperature for several compositions. Again, the point halfway below the knee of the normalized permeability curve was defined as the transition temperature. In Figure III-4 this transition point of $Ni_{1-x}Zn_xFe_{1.95}O_4$ is shown as a function of x for the samples fabricated. In contrast to the iron substitutions in Mn_5Ge_3, we found the transition temperature to be fairly linear with composition changes in the nickel-zinc ferrite system. From this data, the transition temperature was found to change 10°C for a composition change of $\Delta x = 0.007$ in the range between 0 and 100°C.

(1) Resintering

It was obvious that a better method for placing the transition temperature was needed. At best, a predetermined Curie temperature could be achieved within 2°C by controlling the starting composition. Secondly, the mixing procedure is time consuming, and the entire process had to be repeated to obtain a different transition temperature. Some authors (Smit and Wijn, for example) reported zinc losses during the firing procedure. On the basis of this, a series of experiments were performed in the belief that these losses could be controlled, thereby regulating the nickel:zinc ratio that determines the Curie point. We first attempted this by spreading the oxide powders in a thin layer on platinum foil to obtain maximum surface exposure. The powders were fired at 900, 1000, 1100, 1200 and 1300°C for 1 and 2 hours. The results of this testing were inconclusive for two reasons:

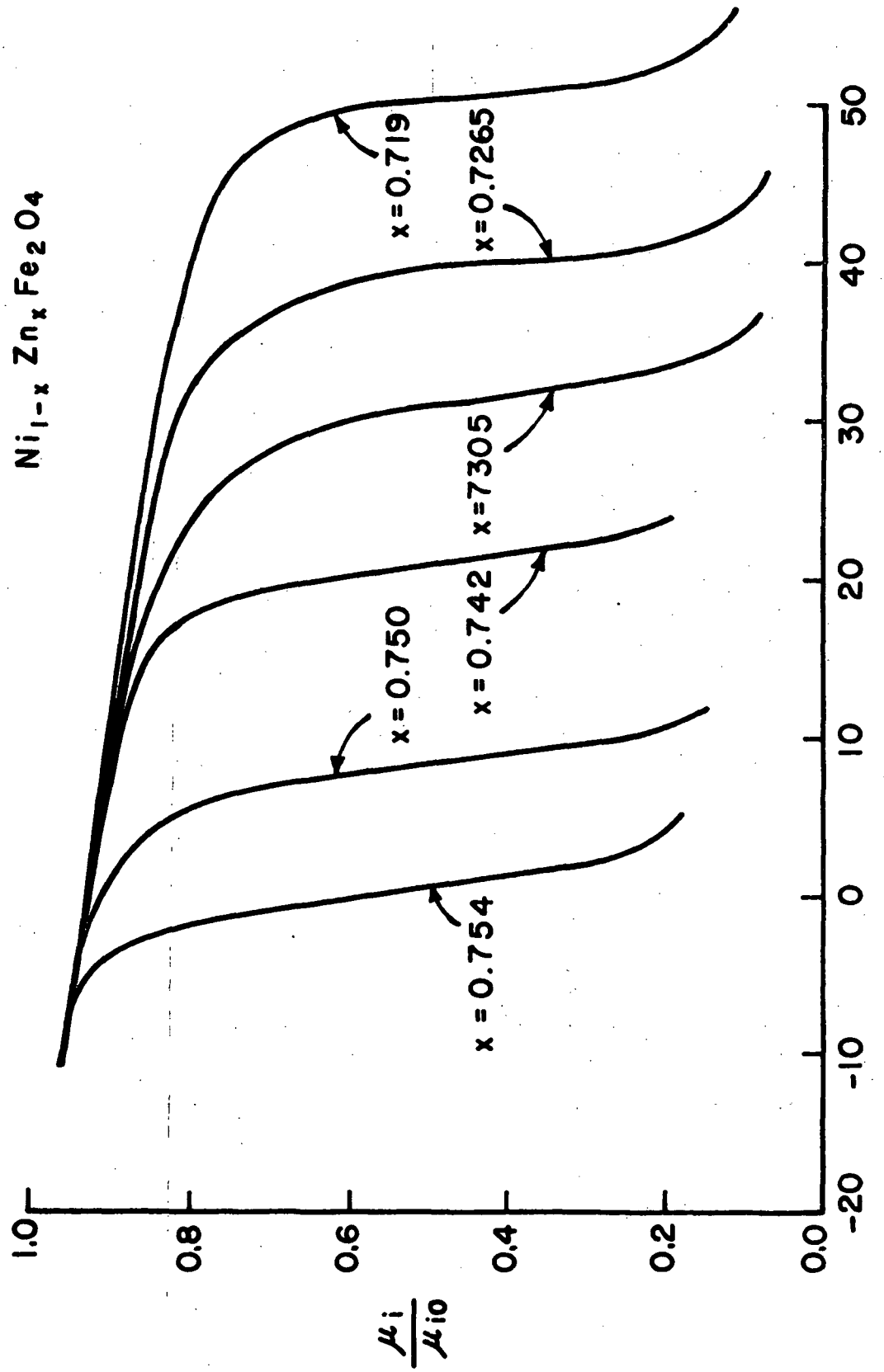

Figure III-3 Normalized permeability versus temperature for several compositions of Ni-Zn ferrite

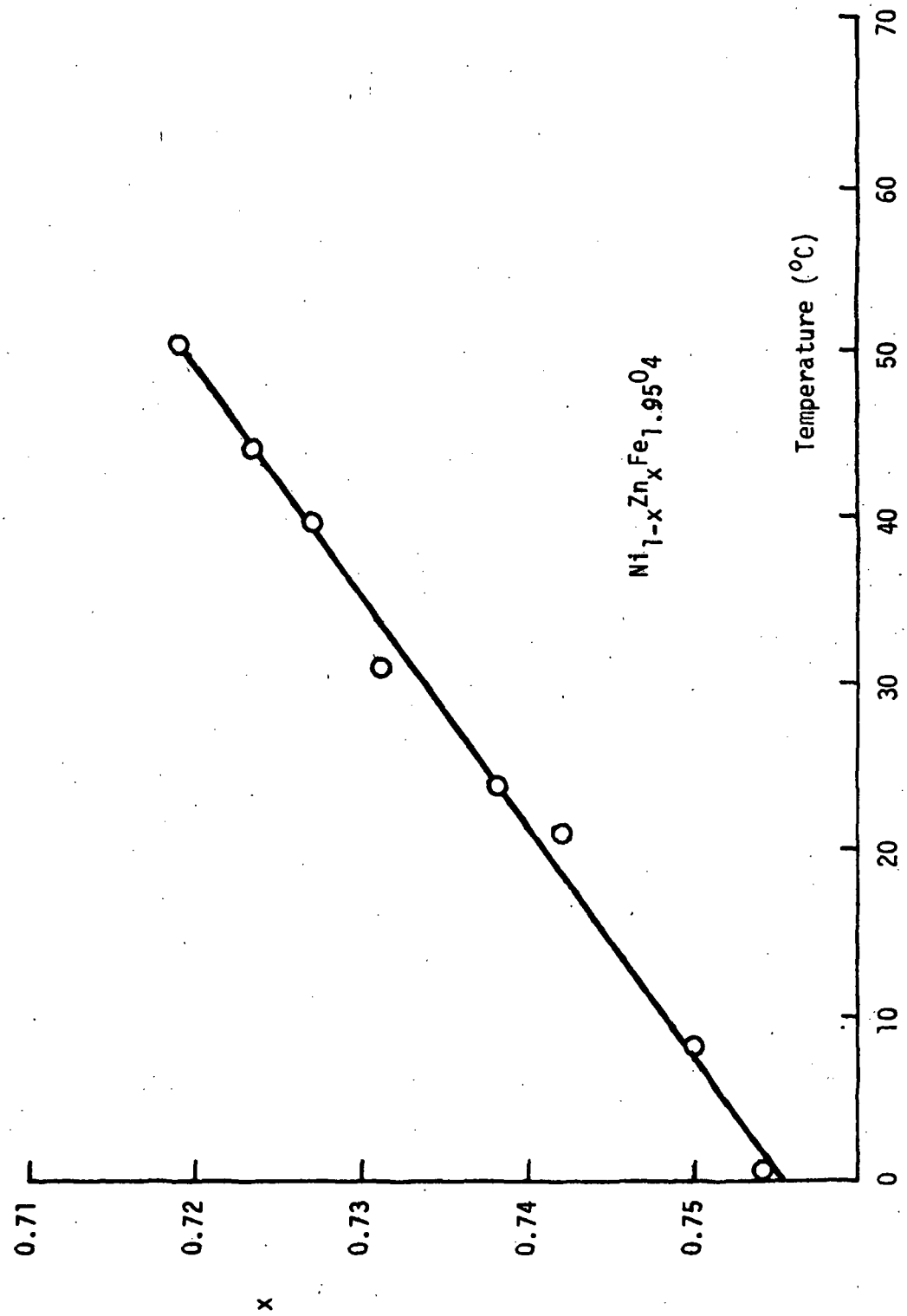

Figure III-4 Transition temperature of Ni-Zn ferrite as a function of zinc concentration

first, the 900 and 1000°C firing temperatures were probably too low to drive off an appreciable amount of zinc; secondly, at the higher temperatures the nickel participates in the reaction and the resulting material was hard and abrasive and extremely difficult to press into a toroid and resinter. An alternate method was to prepare a sample in the usual way (sinter @ 1200°C for 8 hours), measuring the permeability versus temperature characteristics, and then resinter it. If zinc indeed was lost during the second firing, the transition temperature would increase. Figure III-5 is characteristic of the samples prepared in this way. It can be seen that the transition temperature was not affected, but the permeability doubled. We were not able to alter the Curie temperature in this way, but we did verify the fact that the permeability increases with firing temperatures. The higher firing temperature produced a denser sample with a lower porosity. The increase in permeability with density is connected with an increase in the contribution from domain wall displacements. The pores form barriers to prevent or at least hinder the movement of the domain wall.

(2) Nickel Addition

The addition of nickel ions in liquid form to the mixed and dried oxides (see Chapter II), proved to be an effective means of altering the transition temperature. Since the nickel is in liquid form, the composition alterations can be controlled with considerably more accuracy than can the starting composition. Theoretically, since the liquid can be diluted ad infinitum, there is no limit to the incremental shift in Curie temperature in this way. A practical limit, however, is imposed by the measurement apparatus and is approximately 0.1°C. We found that we could change the transition temperature

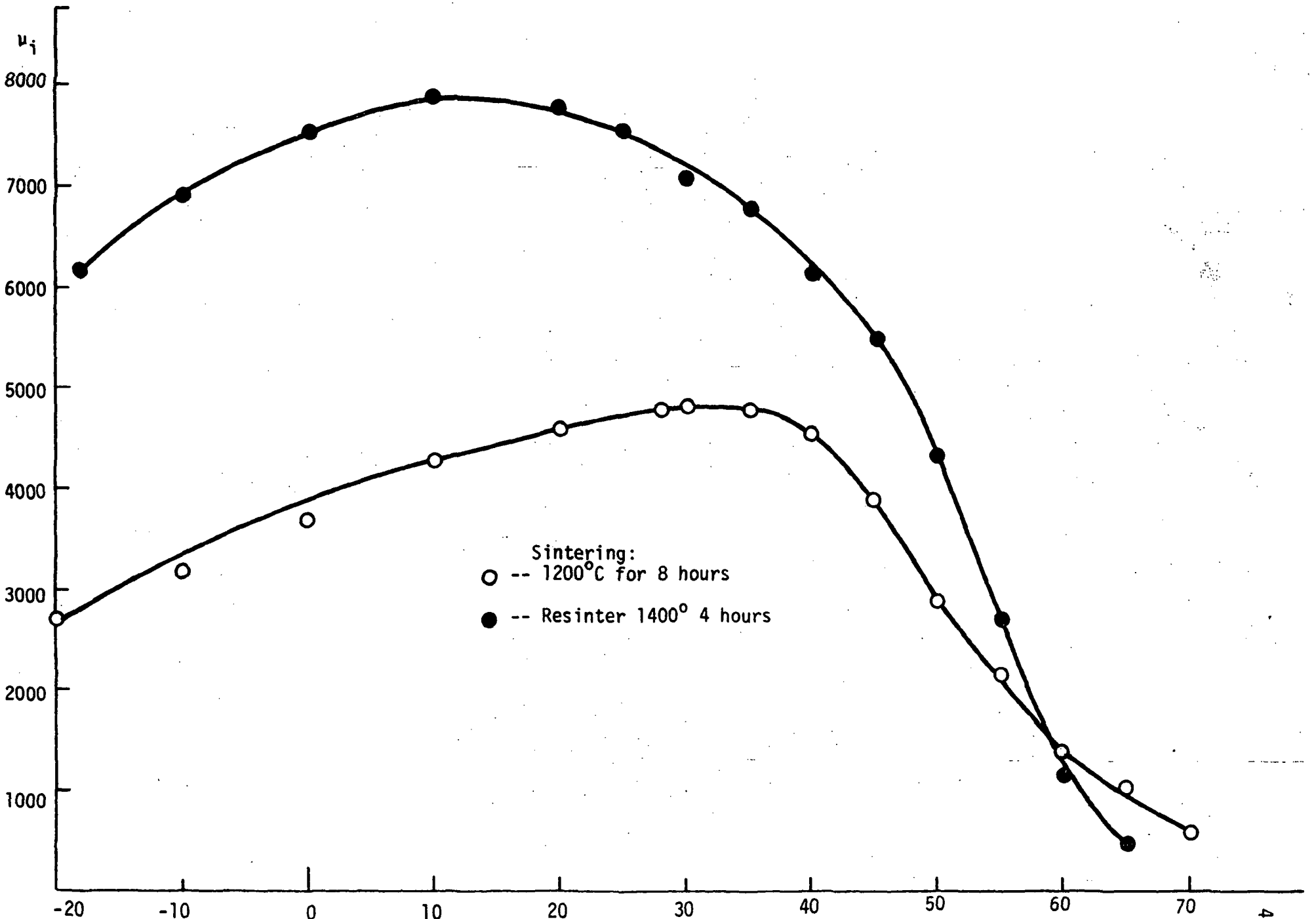

Figure III-5 Permeability versus temperature

(predetermined by the starting composition) up to 10°C higher without affecting the sharpness of the curve on the permeability significantly. Figure III-6 illustrates the effect of composition adjustment in this way. The mid-points of these transitions are depicted as a function of composition change in Figure III-7. Here we show a transition temperature change of 2°C for an effective composition change of x = 0.0015. This corresponds to the composition changes in starting material of 10°C per x = 0.007 shown in Figure III-4. The result is a temperature change of 13.3°C and 14.3°C, respectively, for 1 atomic % composition change in the two methods. The nickel acetate addition results in a fairly linear relation between composition change and Curie point change up to a limit. We found that the transition temperature alterations in this way was limited to approximately 10°C. Further additions of nickel led to a decrease in permeability and smearing of the transition. This suggests the nickel entered interstitially which in effect increased the porosity of the material.

(b) Pulse Measurements

It is important in many applications (See Chapter IV) to utilize the cores as pulse transformers. Therefore, it was necessary to measure the output voltage of the secondary as a function of temperature. Several samples were tested in this way using the circuit in Figure III-8. The input to the primary was a 47 volt, 220 nsec pulse, and the output of the secondary was monitored with an oscilloscope. A 100:1 voltage divider was used to isolate the oscilloscope probe. Either the height of this pulse or of the integrated pulse was measured as a function of temperature. The output pulse is equal to the

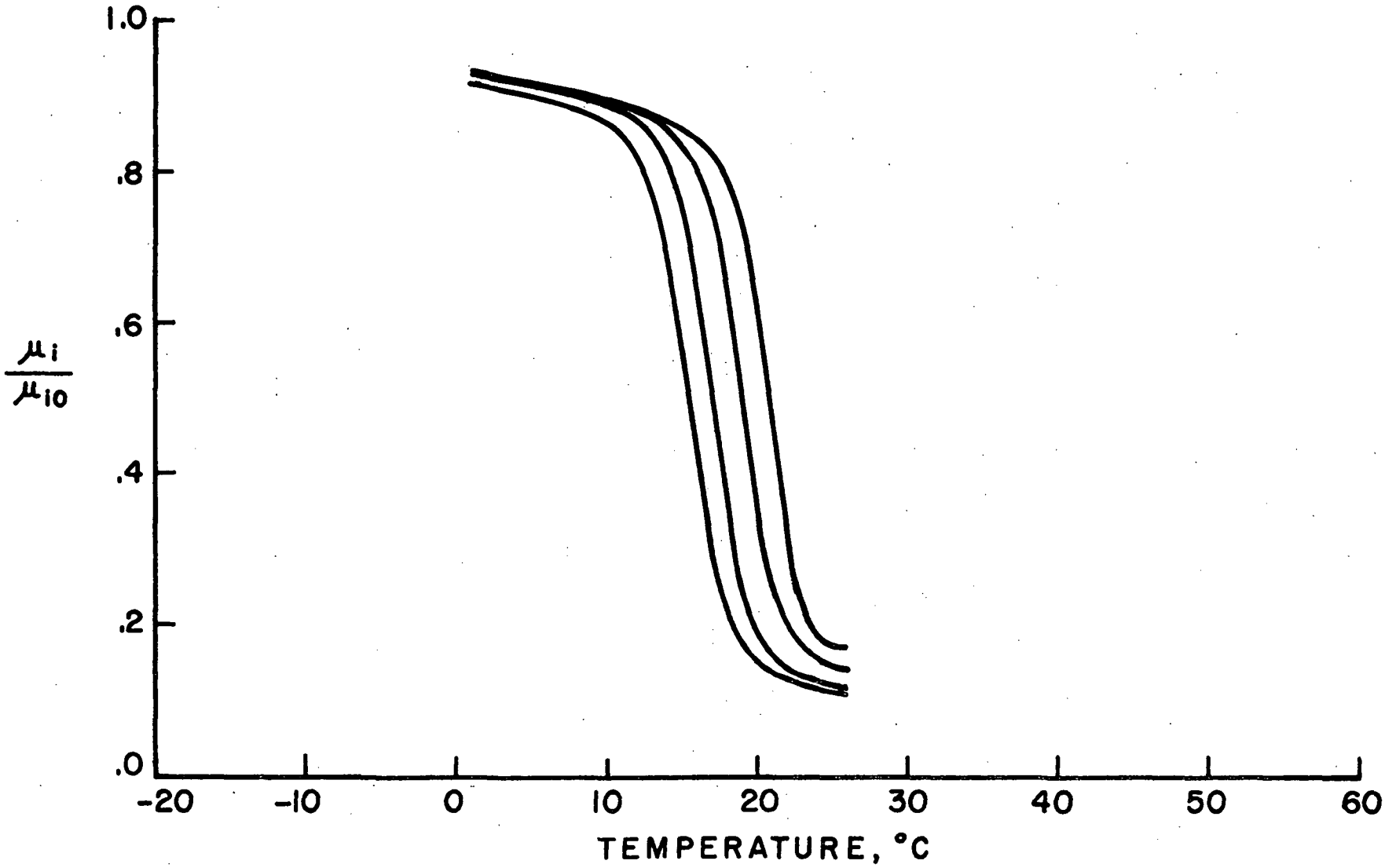

Figure III-8. Normalized permeability versus temperature illustrating nickel acetate addition.

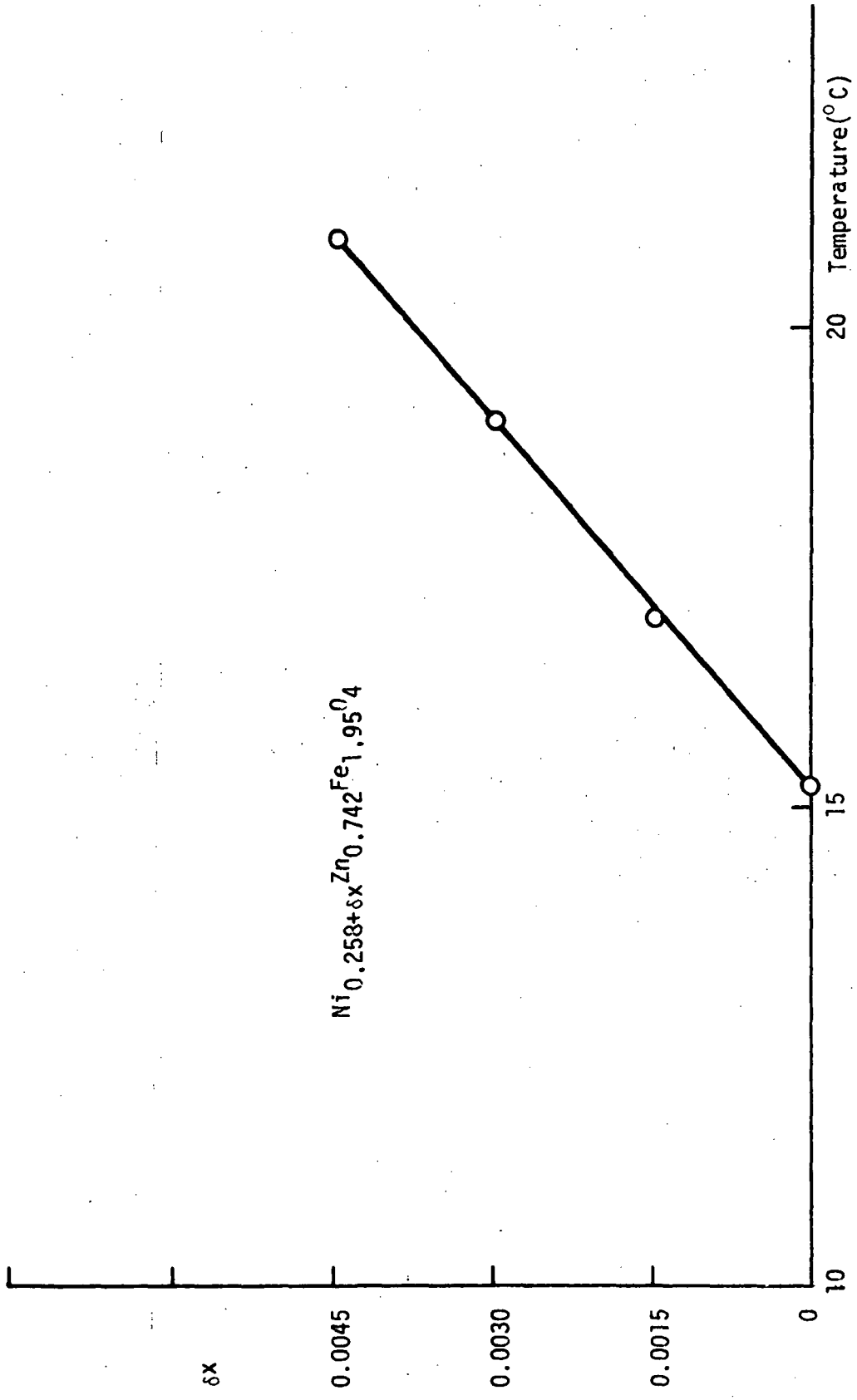

Figure III-7 Shift of transition temperature as a function of nickel doping

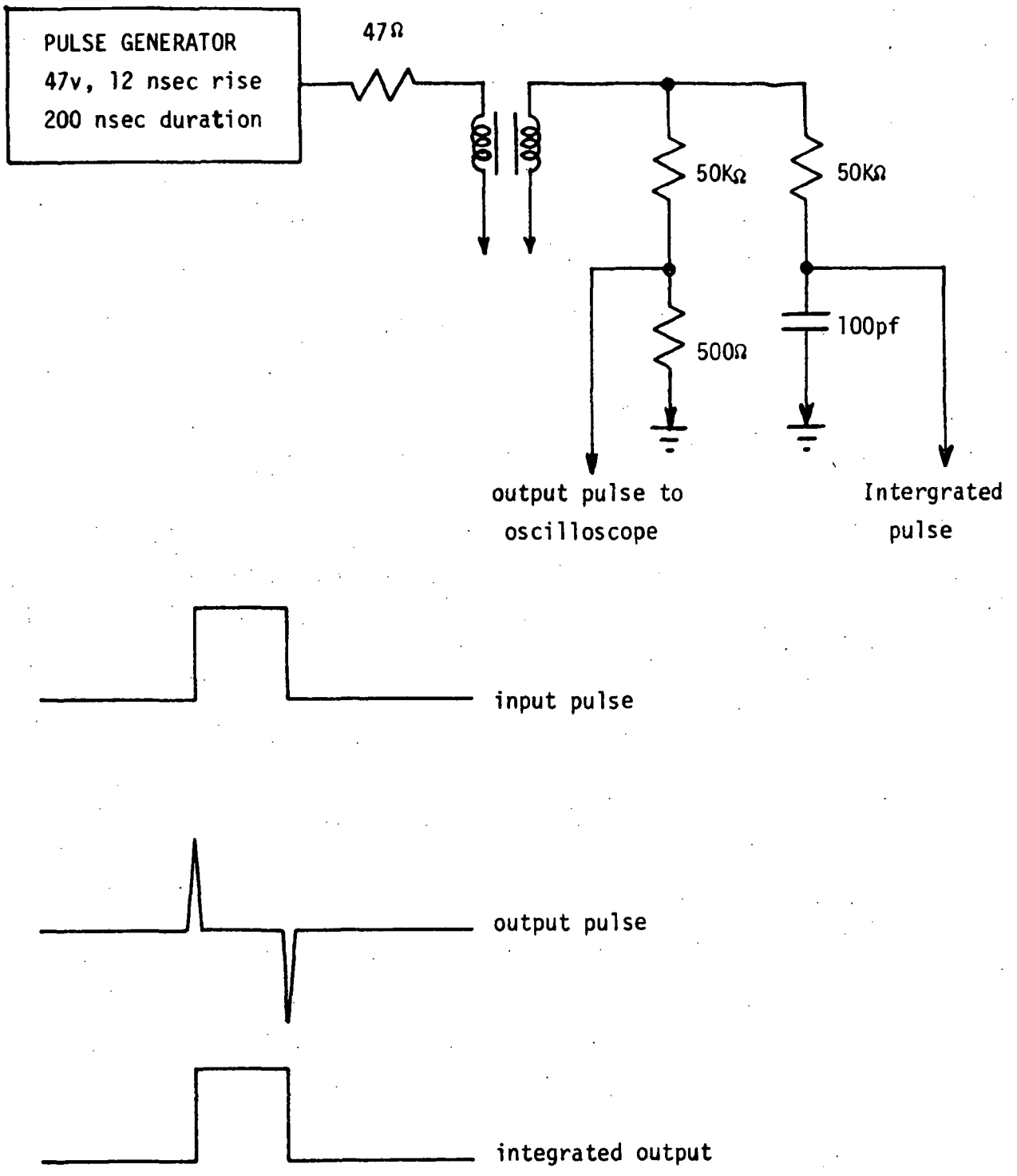

Figure III-8 Circuit and waveforms for pulse measurements

product of the number of secondary turns, N_2, and the time rate of change of the magnetic flux,

For an ideal transformer, the output voltage is

$$V_2 = \frac{N_2}{N} V_1$$

where V_1 is the input voltage to the primary winding of N_2 turns. If the cores are driven into saturation, the output voltage follows the saturation magnetization as a function of temperature. Recall that the saturation magnetization as a function of temperature $M_S(T)$ does not decrease abruptly at the Curie point as does the permeability. We found that when the drive level was decreased sufficiently and the core is not saturated, the coupling is proportional to the permeability. The desired result is that the output pulse decreases abruptly at the transition temperature.

(c) Sine and Triangular Drive

Sinusoidal and triangular current drives were also tested. As with the pulsed input, the drive level must be reduced below the saturation value of the cores. Figure III-9 illustrates the output for various levels of a 5KHz triangular primary current input. At this frequency, the impedance of the transformer ($Z_L = \omega L$) is much less than the 21.5Ω input resistor. Therefore, the input voltage is proportional to the primary current and can be monitored across the input resistor. For triangular drive levels of 0.5 volts peak to peak and less, the core acts as a linear differentiator with the output directly proportional to the permeability. Similar results were obtained with a sinusoidal input.

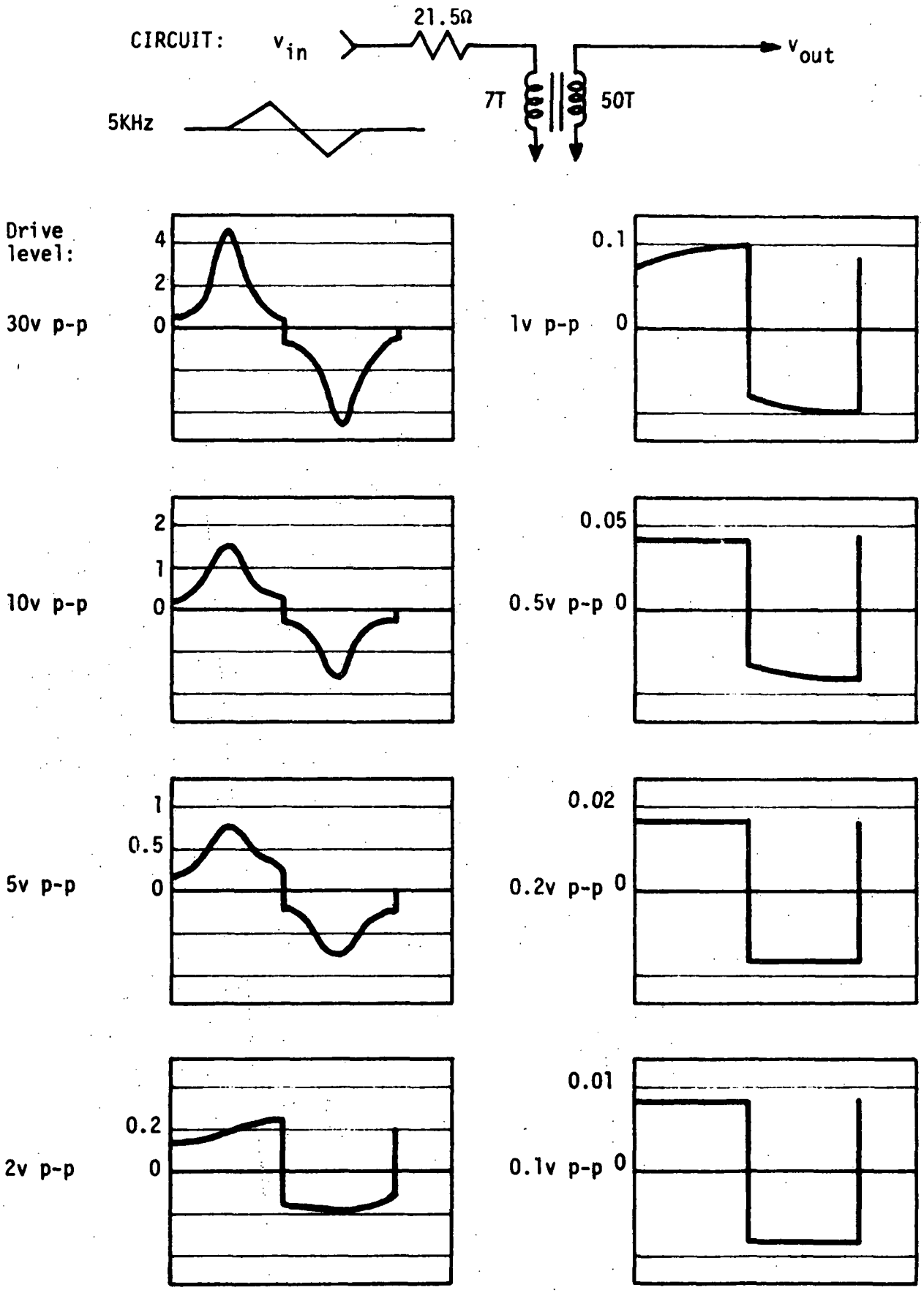

Figure III-9 Output for various levels of triangular current input

(d) Excess Zinc Addition

Ten at. % of zinc was added to the starting composition of a sample of $Ni_{0.2735}Zn_{0.7265}Fe_{1.95}O_4$. The oxides were mixed in the attritor in the usual way and a toroid was sintered at 1200°C for eight hours. Figure III-10 shows the permeability versus temperature for this sample. We prepared a sample in this way for two reasons. First, it was believed that zinc was being lost from the samples during the firing procedure. The additional zinc was added with the possibility of offsetting this loss. Secondly, this sample would yield additional data on zinc addition since the zinc obviously did not enter the structure as a result of zinc acetate addition (see Chapter II). If the zinc:nickel ratio could be increased in the spinel structure in this way, we would observe a decrease in transition temperature from that expected of the original composition. According to Figure III-4, the transition temperature of $Ni_{1-x}Zn_xFe_{1.95}O_4$ for $x = 0.7265$ can be predicted to be approximately 40°C. As shown in Figure III-10, the transition occurs about 42°C. While this 2°C difference is within the experimental accuracy for setting the transition from starting composition, it certainly was not altered to a lower temperature with the addition of extra zinc. However, two interesting observations may be made. The permeability increases slightly before the transition temperature and is characteristic of the properties generally reported for ferrites. This might suggest that a small amount of zinc was indeed lost during the firing of the previous samples. Also, the permeability was considerably lower than previous samples (600 compared to 2000 or 3000).

The obvious conclusion is that the zinc occupied interstitial space and increased the porosity. The same core was also tested as a

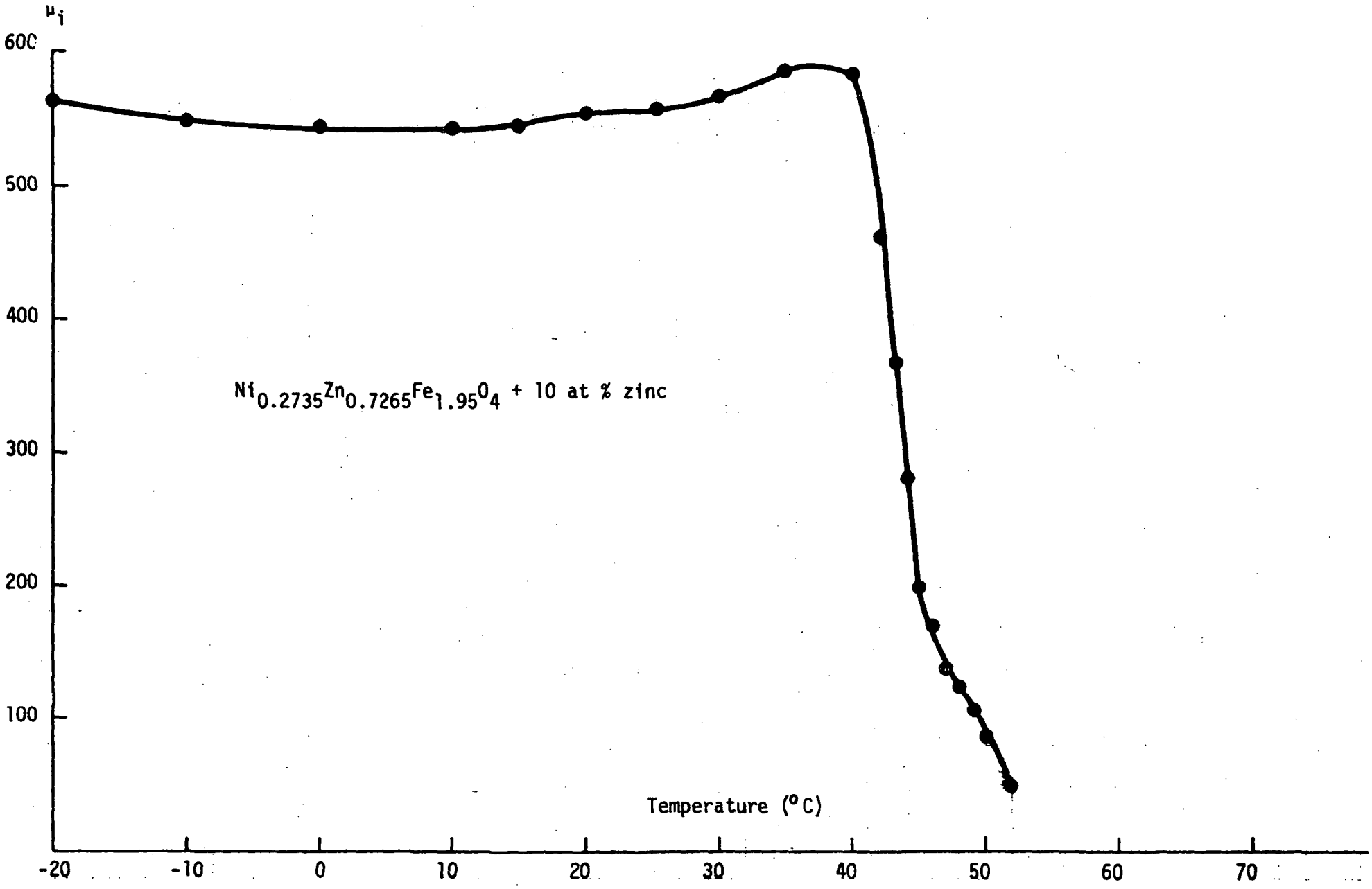

Figure III-10 Permeability versus temperature for 10 at % excess zinc

transformer and the output was measured as a function of temperature. It is worthwhile to note that the output (shown in Figure III-11) decreased abruptly at the transition temperature, but did not have the same small increase in magnitude as did the permeability.

(e) Small Cores

The toroids originally manufactured for testing purposes were too large to be practical for use in a device. This prompted the testing of smaller cores. A machined die similar to that in Figure II-3 was used to produce cores with an average outside diameter of 2.6 mm and inside diameter of 1.6 mm after sintering. This is still far from the state-of-the-art. Commercially, cores are manufactured as small as 1 mil (10^{-3} inches) outside diameter, which is a further reduction in size of about 100. The transitions of these small cores were extremely broad (see Figure IV-12), possibly due to oxygen loss from the lattice. The increased surface to volume ratio with the smaller cores will probably necessitate a different firing procedure. Also, the powders could not be pressed as dense as possible with the larger die. At present, a series of tests are being performed in the Electronic Materials Research Laboratory to determine the correct fabrication procedure for the smaller cores.

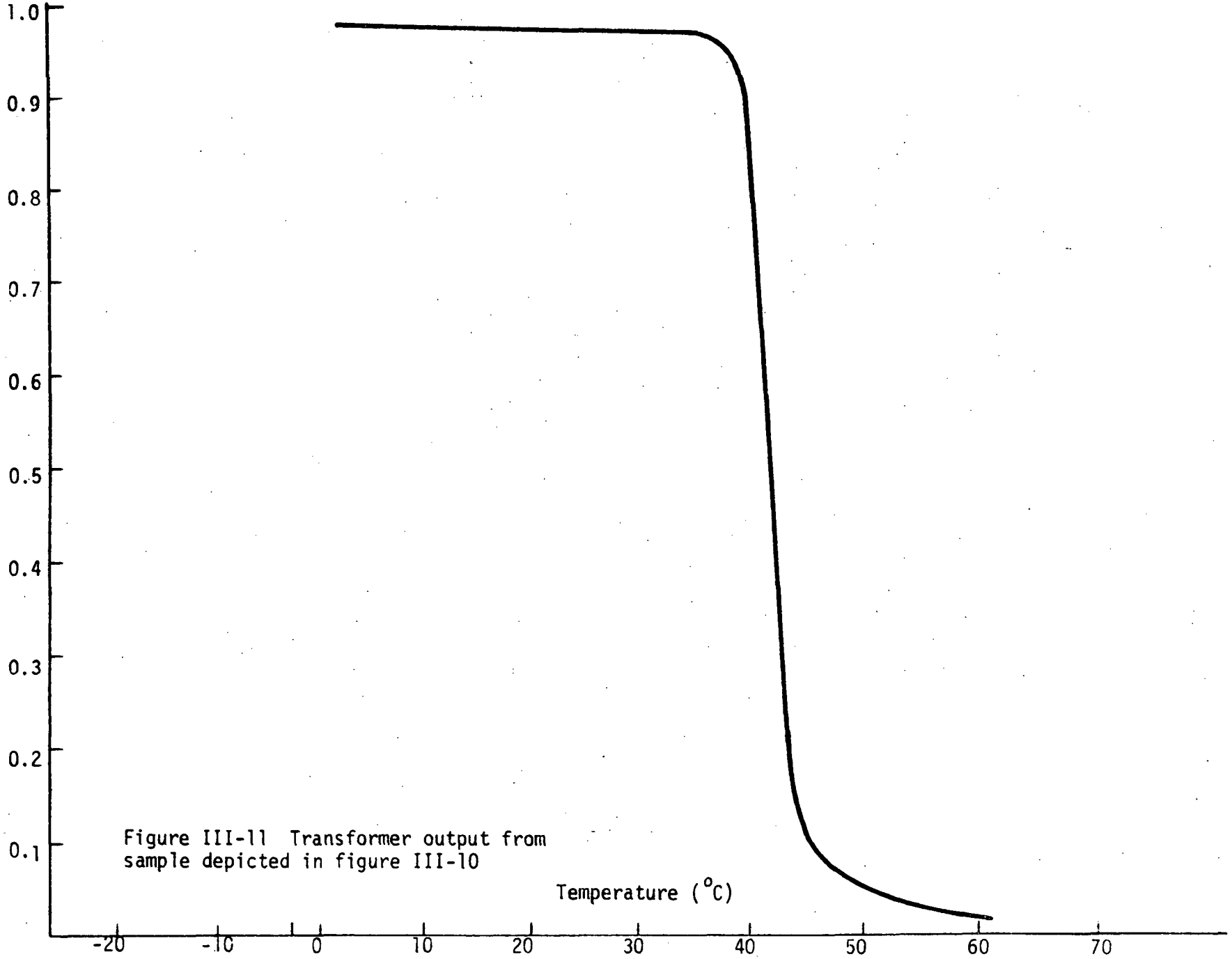

Figure III-11 Transformer output from sample depicted in figure III-10

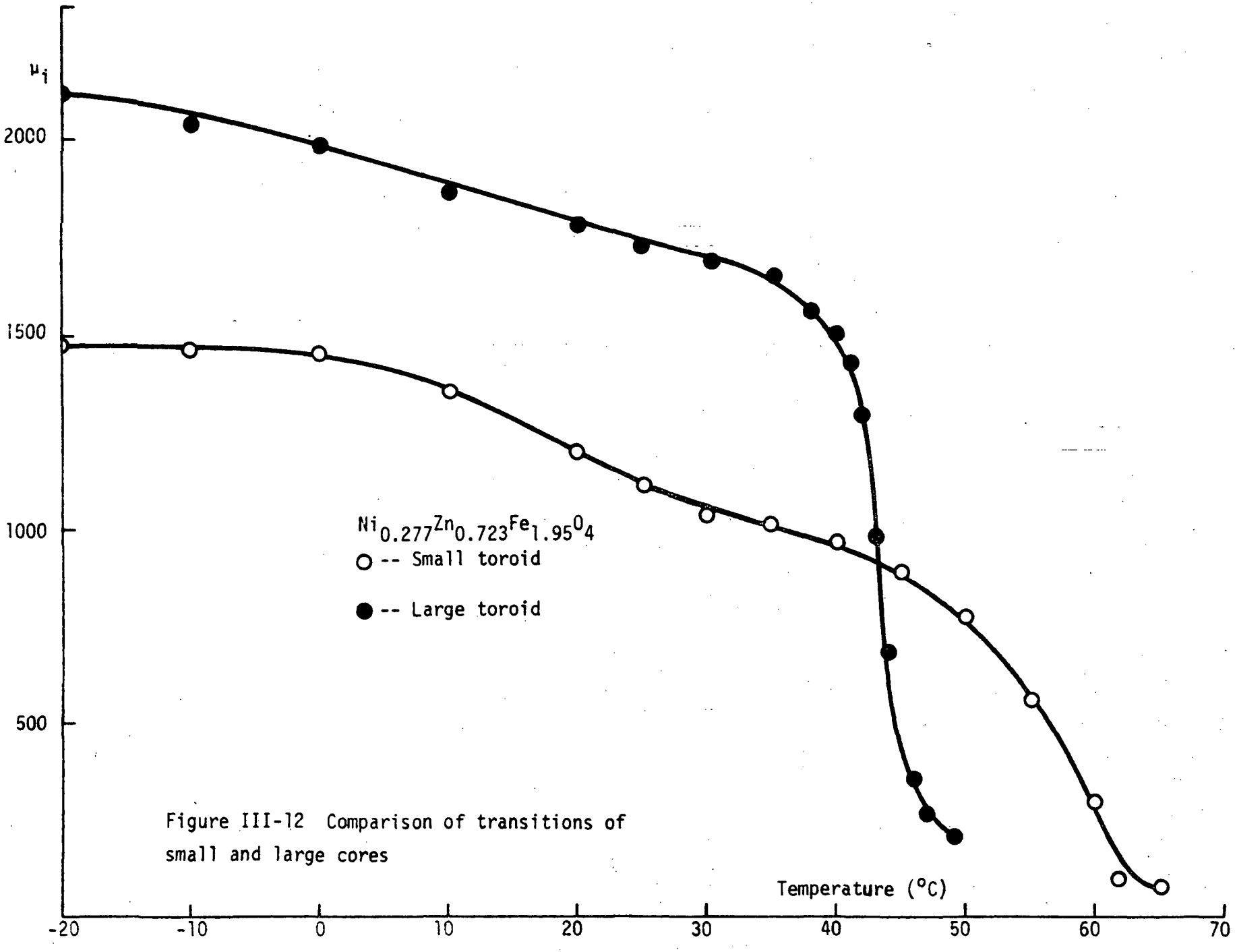

Figure III-12 Comparison of transitions of small and large cores

IV. DEVICES

A. THERMALLY CONTROLLED SWITCH

We have constructed an AC thermally controlled ON-OFF switch without moving parts, using a ferrite toroidal core. The initial permeability controls the AC impedance of a toroidal inductor in series with the load or the mutual coupling between the primary and secondary windings of a toroidal transformer with the load in the secondary. A device similar to that in Figure IV-1A was built and demonstrated at the annual Joint Services visit to The University of Texas at Austin this year.

Below the transition temperature of the toroidal inductor T_1, it appears as a high series impedance and the light bulb B_1 is OFF. Above the transition temperature T_1 is a low series impedance and the bulb is ON. In this manner, the same toroid may be used as a normally-closed switch that changes its state when its temperature passes the Curie temperature. The toroid T_2 and bulb B_2 work analogously, and in addition below the transition temperature, T_2 acts as a transformer and the bulb B_3 is on. Above the transition temperature, there is poor primary to secondary coupling and B_3 is off. Note that B_2 may be replaced by a short circuit without changing the basic operation of B_3 resulting in the device in Figure IV-1B.

The toroidal core T_1 was wound with 30 turns as was the primary of T_2. The number of secondary turns necessary to operate B_3 was determined to be 50 (see below). The 85 KHz sine wave input was supplied by an IC oscillator driving the cores through discrete transistors. If the cores are driven at a low enough level so that the material doesn't saturate, the transformer output or the inductor impedance is proportional to among other things, the driving frequency. The light bulbs were grain of wheat bulbs with an impedance of approximately 50 Ω when operating. For proper operation and to

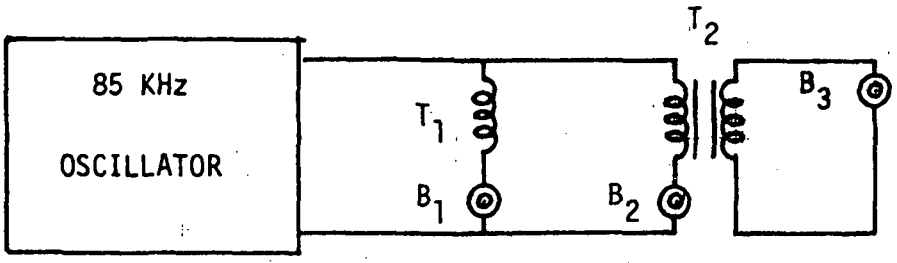

A. ON-OFF switch

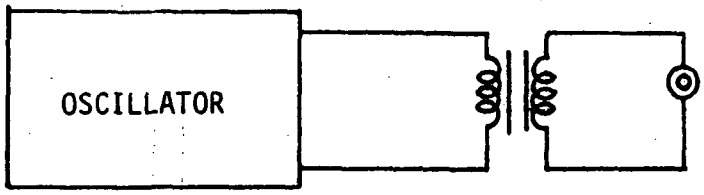

B.

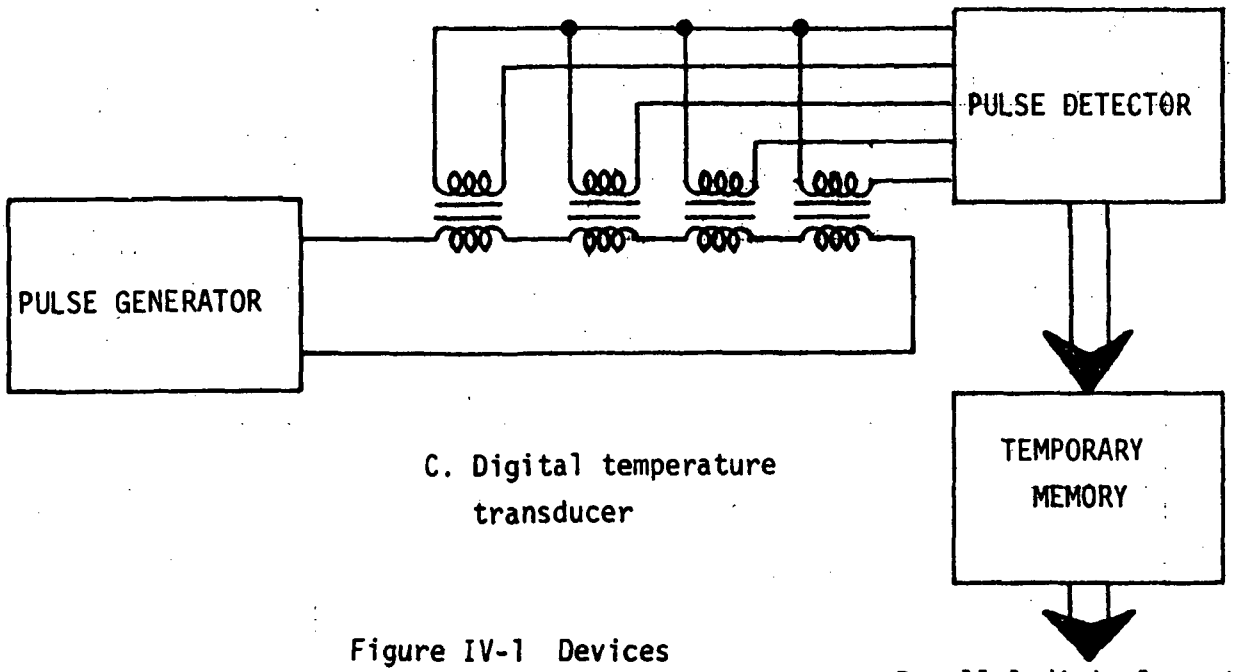

C. Digital temperature transducer

Figure IV-1 Devices

effectively control the lighting of the bulb, the bulb impedance (R) must be approximately that of the inductor (ωL). The resistance of R of the bulb and the inductance of the core are fairly constant; therefore, the driving frequency must be adjusted until proper operation is obtained. This frequency was determined to be 85 KHz. The transformer ratio was then adjusted to achieve proper operation at the same frequency.

B. DIGITAL TEMPERATURE TRANSDUCER

While the ON-OFF switch application is extremely important for cases where the ultimate in reliability is required (no moving parts, radiation insensitive, consisting of only magnetic core and wire, therefore, shock and vibration insensitive with transition temperature determined by chemical composition and, therefore, also not subject to change with time), there exists also an expressed need for a more sophisticated digital transducer which, when interrogated, will deliver a digital output directly related to the temperature of the sensor environment. The proposed device is similar to that shown in Figure IV-1C, and is compatible with digital measurement and control systems. A string of small toroidal cores with transition temperature spaced at a given interval can be interrogated by a current pulse whenever the transducer is addressed by the system. At a given temperature, some of the cores will be below the transition temperature and produce an output pulse, while the rest will be above their transition temperature and will be non-magnetic, therefore producing no output pulses. A simple logic converts the number of pulses from the cores to a digital number recognizable by the control system.

1. Pulse Input

The first step in the design of this device was to identify the different methods of producing a pulsed output from a magnetic sensor and to

define the magnetic properties which are influential in optimizing this pulsed output. The first method attempted is analogous to the interrogation of computer memory cores. In this case, a small toroid core was pulsed with a current interrogation pulse in the primary coil and a pulsed output in the secondary (or sensing) coil will exist only if the core is magnetic, i.e., if it is below its transition temperature. The size of the output pulses in this case is determined by the time rate of change of the magnetic flux in the sensing coil and will, therefore, be related to, among other things, the initial permeability. The peak amplitude of the output pulses is detected to determine if the core is above or below its transition temperature.

One drawback to interrogating the cores in this way is the dependence of peak amplitude of the output pulse on the switching time of the input waveform. Recall that the output of the secondary is the time derivative of the current waveform through the primary (see Figure IV-8). Clearly, variations in rise time of the input waveform will drastically affect the output pulse height. Therefore, in order to utilize this method of interrogation, the output pulse height must be independent of the rise time of the input. Several methods were attempted to accomplish this independence of the output. It was first suggested that the primary be overdriven such that the core material switches between points A and B in its hysteresis loop (see Figure IV-2). If the input rise time is faster than the switching time of the core, the output should depend only on the drive levels (which determines points A and B) and not on the input rise time. We observed an output pulse rise time of less than 10 nsec while the input waveform had a rise time of 12 nsec. Hence, it is not clear that the switching time of the core is yet the limiting factor.

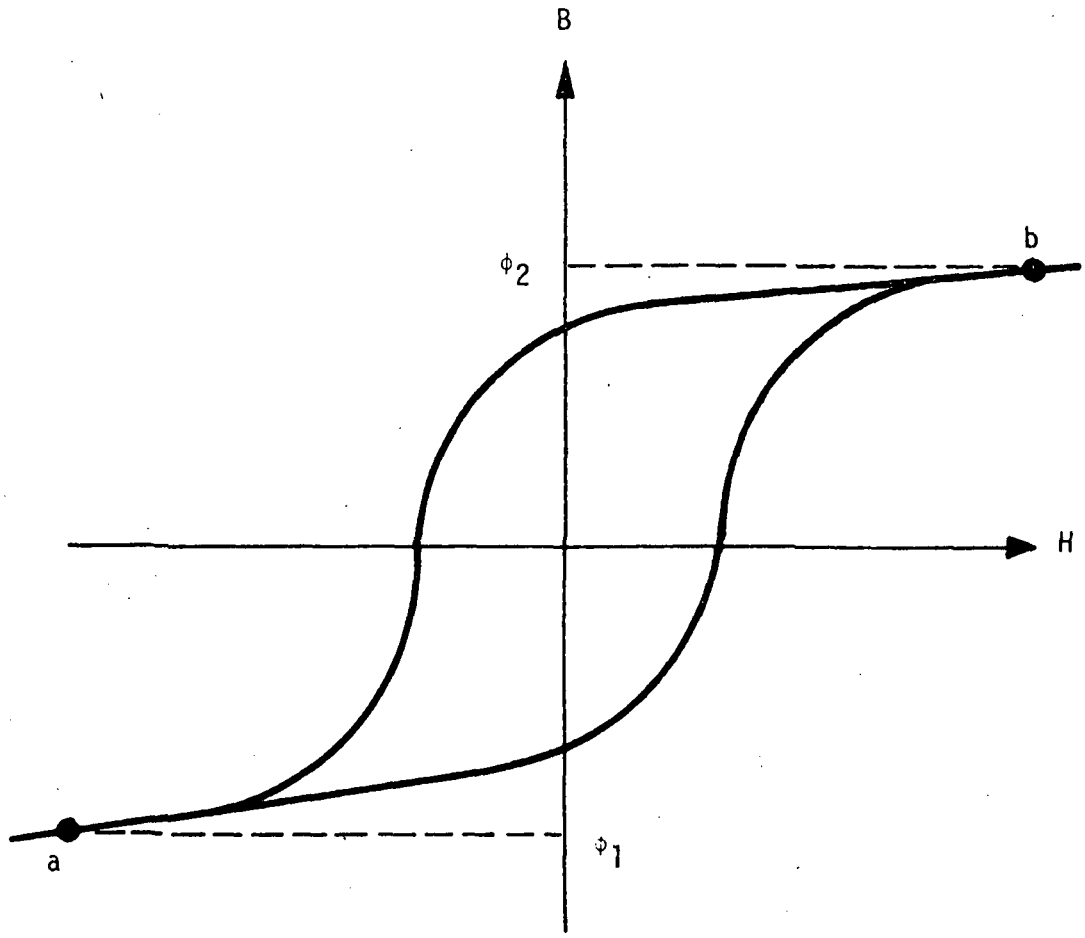

Figure IV-2 Typical hysteresis loop for ferrite cores

An alternate method is to integrate the output pulse of the sensing coil. The area under the output pulse should be independent of the input rise time and depend only on the difference between the final flux values in the core $(\phi_1 - \phi_2)$.

This corresponds to the values illustrated in Figure IV-2 at points a and b, respectively. The main objection to both these methods is the fact that the material is driven into saturation. If the cores are saturated, the output voltage as a function of temperature follows the saturation magnetization which is a monotonic function of temperature and not the initial permeability which is discontinuous (see Chapter III). A further objection to the second method is the signal loss if passive integration is used. For RC integration, the value of the RC time constant must be much greater than the width of the output pulse to be integrated. Since there is a limit to the current the secondary coil can deliver, there is a lower limit on the value of resistance that can be used in the circuit. Therefore, most of the voltage is dropped across this current limiting resistor. For R = 47K Ω and C = 100 pf, we observed a factor of 20 in signal loss when an effective integration was achieved using discrete components. If, on the other hand, active integration is attempted, the fast rise times involved prohibit the use of all but the most sophisticated operational amplifiers.

2. Triangular Input

The main thing to bear in mind is the fact that the device must utilize the discontinuous permeability versus temperature characteristics. Therefore, the transducer must operate as a linear transformer and the material cannot be driven into saturation. A linear transformer has a transfer function directly proportional to the permeability. This fact, among others, led to the investigation of different types of input waveforms. Since the

transformer is a differentiator, a triangular current input will give a square wave voltage output. In addition, there is no longer a dependence on the rise time of an input pulse. Experiments confirmed that a square wave output could be obtained for a triangular input at low levels (see Figure III-9)

3. Output Detection

The desirable characteristics of the sense portion of the interrogation are:

(1) Low threshold voltage level.

(2) Threshold stable with temperature since the logic and cores may be at different temperatures.

(3) Voltage compatibility with other logic circuitry.

a. power supply compatibility

b. logic level compatibility

(4) A small number of IC packages. Assuming that the amplitude of the output follows the permeability as a function of temperature, then the discontinuity of the output levels at the transition temperature can be quantized by means of:

a. IC comparators

b. IC Schmitt trigger

c. emitter coupled logic (ECL)

d. sense amplifiers

Comparators can be used with lower output levels which would reduce the number of secondary turns necessary, but they require a negative voltage for operation and a voltage reference with which to compare the output pulse height. In addition, there are only two comparators per IC package available. IC Schmitt triggers are voltage level compatible with other logic of the same

family, require only a single power supply, and have a threshold level which is more stable than a gate input. But, on the other hand, Schmitt triggers generally are not as stable as comparators. There are two to four IC packages available. The number of secondary turns can also be minimized by utilizing the low voltage swing of 0.8 volt between "1" and "0" of emitter coupled logic. The 0.8 volt between "1" and "0" is attractive, and some new ECL families have characteristics which are as stable versus temperature as Schmitt triggers of saturating logic families. The drawback is that ECL is not as popular as other families of digital logic, thus necessitating additional interface circuitry to make the logic levels compatible. Sense amplifiers require the smallest input voltage levels of these four types for operation, but are available in only one to two per package and require a negative voltage supply as well.

C. Other Devices

Other applications using the change in inductance with temperature were considered. While not requiring an excess of additional circuitry, they have considerably more sensitivity. For example, if the inductor is part of a balanced bridge, temperature changes of less than 0.001°C will unbalance the bridge significantly in the region of the transition.

If the inductor is used in an oscillator circuit, the change in oscillating frequency can be used to detect variations in temperature on the order of 10^{-5} to 10^{-6} degrees, thus demonstrating an extremely sensitive bolometer with no need for calibration. One possible use might be a sensitive infrared detector without cryogenic cooling.

D. Recommendations for Additional Research

We have been able to shift the transition temperature of the ferrites up to 10°C higher than the temperature determined by the starting composition

by adding nickel ions in liquid form. It was expected that zinc additions in this way would lower the transition temperature, but to date this has been unsuccessful. Obviously, a much greater flexibility in temperature range would be achieved if a process for lowering the transition temperature could be implemented. At least 20°C range of transition temperatures (10° above and 10° below) would be possible from any given starting composition. Further experimentation with the addition of nickel and zinc ions in liquid form could lead to an even larger range of temperatures available with a given starting mixture.

For device applications, it is necessary to reduce the size of the cores. Fabrication techniques must be perfected such that the smaller cores have a sharp transition that can be utilized for temperature detection. The smaller size not only reduces the dimensions necessary for the device, but the smaller mass enables the core to follow small temperature deviations with increased sensitivity.

The design considerations listed above for the digital temperature transducer represent a small amount of the thought that has gone into this device. Many of the details need to be worked out to realize a working device. Most of the design is now complete and the logic is being breadboarded. Further testing of the design is necessary to establish the electronics necessary to achieve a given repeatability and quality.

APPENDIX A

When a material with high permeability ($\mu >> \mu_0$) is fabricated into a toroid and has a uniform winding of many turns, flux leakage can be neglected and the flux lines are confined almost entirely inside the winding. If $\frac{2R}{a} >> 1$ (see Figure A-1), the flux linkages are

$$\Lambda = N\phi = NBA = NBab \qquad [1]$$

where A = ab is the cross sectional area of the toroid. Since $B = \frac{\mu NI}{\ell}$, we have

$$\Lambda = \frac{\mu N^2 I ab}{\ell} \qquad [2]$$

where I is the current through the winding and ℓ is the length of the flux path. The flux path is $2\pi R$, therefore

$$\Lambda = \frac{\mu N^2 I ab}{2\pi R} . \qquad [3]$$

The inductance of the toroid is then

$$L = \frac{\Lambda}{I} = \frac{\mu N^2 ab}{2\pi R} . \qquad [4]$$

The permeability of the material is

$$\mu = \frac{2\pi RL}{N^2 ab} \qquad [5]$$

where μ = permeability (henrys/meter)

L = inductance of toroid (henrys)

R = radius of toroid (meters)

N = number of turns

ab = cross sectional area of toroid (meters^2).

It was desirable to know the relative permeability, therefore

$$\frac{\mu}{\mu_0} \text{ (dimensionless)} = \frac{RL}{ab} (2 \times 10^3) \qquad [6]$$

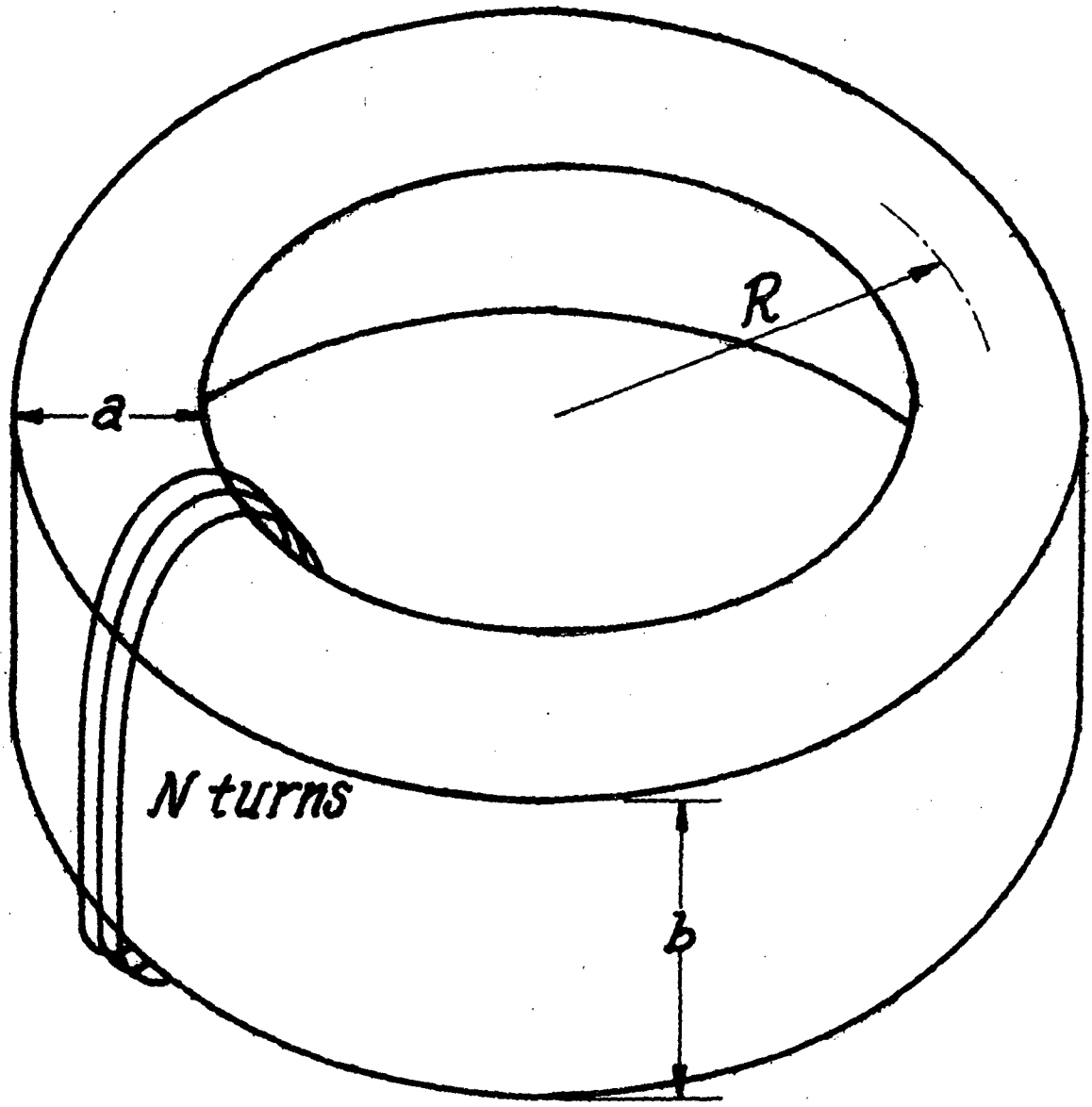

Figure A-1 Toroidal shape

where μ_o is the permeability of free space ($4\pi \times 10^{-7}$ henry/meter) and N = 50 for the test cores. The physical size was determined in mm with a micrometer (accuracy $\pm$ 0.05 mm) by measuring the inside diameter (ID), the outside diameter (OD) and the thickness (b) of the toroids. Since R = 1/2 ID + $\frac{OD - ID}{4}$ and a = $\frac{OD - ID}{2}$, the constant $\frac{R}{ab}$ was easily determined. The inductance was measured in micro-henrys, thus the following formula was computed for direct conversion from inductance to μ/μ_o:

$$\frac{\mu}{\mu_o} = \left(\frac{OD + ID}{OD - ID} \frac{1}{2b}\right) 2 \times 10^3 L \qquad [7]$$

where OD, ID, and b are measured in mm and L is measured in micro-henrys.

Above the Curie point, the material is paramagnetic and the permeability is equal to that of free space. The inductance of the core will be the same as that of an air core of the same dimensions. This value of inductance (L_o) can be calculated from Eq. [4] by substituting μ_o for μ. The relative permeability may, therefore, be determined by an alternate relation

$$\frac{L_m}{L_o} = \frac{\mu}{\mu_o} \qquad [8]$$

where L_m is the inductance measured at any given temperature.

REFERENCES

1. Wang, Shyh, Solid State Electronics, p. 456, McGraw-Hill Book Company, New York (1966).
2. Soohoo, Ronald F., Theory and Application of Ferrites, p. 36, Prentice-Hall, Inc., New Jersey (1960).
3. Standley, K.J., Oxide Magnetic Materials, p. 1, Oxford University Press, London (1962).
4. Wang, ibid., p. 460.
5. Weiss, P., J. Physics, 6, p. 667 (1907).
6. Standley, ibid., p. 2.
7. Zwicker, U., E. Jahn and K. Schubert, Z. Metallkde, 40, p. 433 (1949).
8. Castelliz, L., Monatsh. Chem., 84, p. 765 (1953).
9. Ch. Guilland, C.R., Rev. Mod. Physics, 25, p. 119 (1953).
10. Reiff, W.M., K.S.V.L. Narasimhan and H. Steinfink, to be published.
11. Tawara, Yoshio and Kiyoo Sato, Journal of the Physical Society of Japan, 18, p. 773 (1963).
12. Wang, ibid., p. 489.
13. Fresh, Donald L., Proc. of IRE, p. 1303, October (1956).
14. Standley, ibid., p. 20.
15. Wang, ibid., p. 490.
16. Bates, L.F., Modern Magnetism, p. 49, Cambridge University Press (1951).
17. Morrish, Alan H., The Physical Principles of Magnetism, p. 504, John Wiley and Sons, New York (1965).
18. Neél, L., Ann. de phys., 3, p. 137 (1948).
19. Gorter, E.W., Phillips Res. Rept., 9, p. 295 (1954).
20. Smit, J. and H.P.J. Wijn, Ferrites, p. 153, John Wiley and Sons, New York (1959).

21. Standley, *ibid*, p. 63.

22. Soohoo, ibid., p. 36.

23. Chikazumi, Sōshin, Physics of Magnetism, p. 124, John Wiley and Sons, New York (1964).

24. Wijn, W.P.J. and J.J. Went, Physica, 17, p. 976 (1951).

25. Rathenau, G.W. and J.F. Fast, Physica, 21, 964 (1955).

26. Guilland, C.,Proc. Inst. Elec. Engrs. (London), 104B, p. 165 (1957).

27. Galt, J.K., Physical Review, 85, 664 (1952).

28. Smit and Wijn, ibid., p. 250.

29. Latimer, Wendell M. and Joel H. Hildebrand, Reference Book of Inorganic Chemistry, p. 130, The MacMillan Co., New York (1946).

30. Private communication with Dr. Hugo Steinfink.

31. Instruction Manual for Union Process, Inc., Research Model Attritor #01.

32. Smit and Wijn, ibid., p. 157.

33. Van Uitert, L.G., J. Chem. Phys., 23, p. 1883 (1955).